



# A class of nonconforming immersed finite element methods for Stokes interface problems

Derrick Jones<sup>a</sup>, Xu Zhang<sup>b,\*</sup>

<sup>a</sup> Department of Mathematics and Statistics, Mississippi State University, Mississippi State, MS 39762, United States of America

<sup>b</sup> Department of Mathematics, Oklahoma State University, Stillwater OK 74078, United States of America



## ARTICLE INFO

### Article history:

Received 7 March 2020

Received in revised form 13 November 2020

### Keywords:

Immersed finite element  
Stokes interface problem  
Nonconforming finite element  
Crouzeix–Raviart  
Rotated  $Q_1$

## ABSTRACT

In this paper, we introduce a class of lowest-order nonconforming immersed finite element (IFE) methods for solving two-dimensional Stokes interface problems. The proposed methods do not require the solution mesh to align with the fluid interface and can use either triangular or rectangular meshes. On triangular meshes, the Crouzeix–Raviart element is used for velocity approximation, and piecewise constant for pressure. On rectangular meshes, the Rannacher–Turek rotated  $Q_1$ – $Q_0$  finite element is used. The new vector-valued IFE functions are constructed to approximate the interface jump conditions. Basic properties including the unisolvency and the partition of unity of these new IFE functions are discussed. Approximation capabilities of the new IFE spaces for the Stokes interface problems are examined through a series of numerical examples. Numerical approximations in the  $L^2$ -norm and the broken  $H^1$ -norm for the velocity and the  $L^2$ -norm for the pressure are observed to converge optimally.

© 2021 Elsevier B.V. All rights reserved.

## 1. Introduction

Many physical phenomena involve multiple materials and mathematicians often model these phenomena by partial differential equations with material interface. The solutions to these interface problems often exhibit kinks, discontinuities, singularities, and other non-smooth behaviors. In recent decades, developing efficient and accurate numerical methods for solving interface problems has received wide attention. Conventional numerical methods such as the finite element method (FEM) [1,2] often require the solution meshes to align with material interfaces, i.e., to use an interface-fitted mesh, otherwise, the approximation may not be accurate if not worse [2]. On the other hand, to have the mesh to fit the interface requires constantly re-meshing as the interface evolves with time, which is often computationally expensive. Many efforts have been made to solve interface problems without the aligning requirement, i.e., to solve interface problems on unfitted meshes. See Fig. 1 for an illustration of these two types of meshes.

The immersed finite element method (IFEM) is one of these unfitted-mesh methods. The main idea of IFEM is to locally modify the approximation function around the interface to accommodate the interface jump conditions. In [3], Li introduced the piecewise linear IFEM for one-dimensional elliptic interface problems. Since then many articles have been published in extending this method to higher-order approximations [4–6] and multi-dimensional interface problems [7–12]. Besides, the IFEM has been applied to other interface problems including parabolic interface problems [13,14], hyperbolic interface problems [15,16], shape optimization inverse problems [17,18], elasticity interface problems [19–21], moving interface problems [22,23], triple-junction interface problems [24,25], and plasma simulations [26,27].

\* Corresponding author.

E-mail addresses: [djt70@msstate.edu](mailto:djt70@msstate.edu) (D. Jones), [xzhang@okstate.edu](mailto:xzhang@okstate.edu) (X. Zhang).

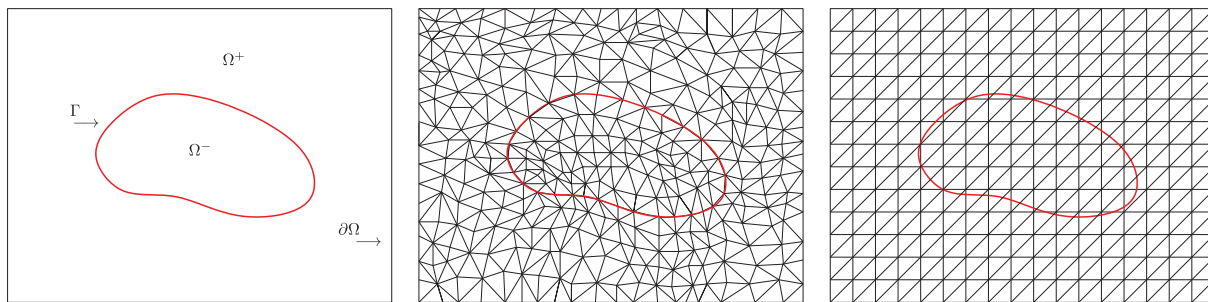


Fig. 1. From left: the domain of an interface problem, an interface-fitted mesh, and an unfitted mesh.

Stokes equations are used to model multiphase flow with jumps in velocity, pressure, and physical parameters. There have been a few numerical methods based on unfitted meshes for Stokes equations including CutFEM [28], Nitsche’s Extended FEM [29], XFEM [30], fictitious domain FEM [31,32], immersed interface method [33], etc. As for IFEM, Adjerid, Chaabane, and Lin developed an immersed  $Q_1$ - $Q_0$  discontinuous Galerkin (DG) method [34]. The velocity vector is approximated by the broken  $Q_1$  functions while the pressure is approximated by the piecewise constant functions. This discontinuous IFE space is stable and the corresponding immersed DG method is observed to have optimal convergence in both the velocity and the pressure.

In this paper, we develop two IFE approximations for the steady-state Stokes equations. Our methods are based on the nonconforming FEM framework. It is well-known that the nonconforming  $P_1$  finite element, widely known as Crouzeix–Raviart (CR) element [35] defined on triangular meshes and the nonconforming  $Q_1$  element, known as Rannacher–Turek element [36] or the rotated- $Q_1$  ( $RQ_1$ ) element defined on rectangular meshes are both stable finite element pairs for Stokes equations [37,38]. Comparing with the Taylor–Hood finite element [39], these nonconforming finite elements can use low-order polynomials and they are element-wise divergence-free [40].

The proposed IFE methods locally modify the CR- $P_0$  and the  $RQ_1$ - $Q_0$  FE basis functions on interface elements. Trying to keep the original FE structure as much as possible, we use standard FE basis functions on non-interface elements. On interface elements, we construct new basis functions to incorporate the interface jump conditions. Unlike the Poisson equation [41], the IFE basis functions on interface elements are vector-valued since the stress interface condition (2.7) couples together the velocity and the pressure variables. The vector-valued IFE basis functions have been developed for the elasticity system in [20,21] and for the Stokes equation in [34]. Comparing to other unfitted-mesh FEMs [28–30], the proposed IFE spaces are isomorphic to the standard CR- $P_0$  or  $RQ_1$ - $Q_0$  FE spaces on the same mesh. In other words, the number and the location of the degrees of freedom of the IFE space are identical to the corresponding FE space as if there were no interface. This structure-preserving feature is desirable in solving a moving interface problem [22] and can also adopt existing fast solvers from standard FEM.

Comparing with the  $Q_1$ - $Q_0$  IDG method [34], the computation cost for the proposed IFE methods is significantly less. To be more specific, on a Cartesian mesh with  $N \times N$  rectangles, the  $Q_1$ - $Q_0$  IDG method has  $9N^2$  degrees of freedom, but the new  $RQ_1$ - $Q_0$  IFEM has only  $5N^2$  degrees of freedom. Cutting each rectangle into two triangles, our new CR- $P_0$  IFEM has  $8N^2$  degrees of freedom, still less than the IDG method. Another difference is in the numerical algorithm. Since the IDG method does not enforce continuity across the elements, the computational algorithm must contain additional consistency and stability terms. However, our nonconforming IFE spaces impose weak continuity such that the average integral value across the edges is continuous [41,42]. There is no need to include these additional terms in our numerical scheme. Thus, the new IFE algorithm has a much simpler form comparing to the IDG scheme in [34]. The proposed nonconforming IFE method is probably one of the simplest unfitted-mesh methods for Stokes interface problems.

The rest of the paper is organized as follows. In Section 2, we present the steady-state Stokes interface problems and introduce some preliminary notations. In Sections 3 and 4, we construct the CR- $P_0$  and  $RQ_1$ - $Q_0$  IFE spaces on triangular and rectangular meshes, respectively. In Section 5, we present some fundamental properties of the new vector-valued IFE spaces, including unisolvency, consistency, and partition of unity. In Section 6, we derive the weak formulation of the Stokes interface problem and present the nonconforming IFE method for this problem. In Section 7, we report some numerical examples to demonstrate the optimal approximation capability of the IFE spaces and the corresponding IFE solutions. Brief conclusions will be given in Section 8.

## 2. Stokes interface problems

We are interested in steady-state fluid flow problems consisting of two immiscible fluids separated by an interface. Let  $\Omega \subset \mathbb{R}^2$  be an open bounded domain separated by a smooth interface  $\Gamma$ . The interface  $\Gamma$  separates  $\Omega$  into two disjoint subdomains  $\Omega^+$  and  $\Omega^-$  such that  $\bar{\Omega} = \bar{\Omega}^+ \cup \bar{\Omega}^-$  and  $\Omega^+ \cap \Omega^- = \emptyset$ . Each subdomain is occupied by a fluid. See Fig. 1 for an illustration of the domain. Consider the governing incompressible Stokes equations:

$$-\nabla \cdot S(\mathbf{u}, p) = \mathbf{f} \quad \text{in } \Omega^+ \cup \Omega^-, \tag{2.1}$$

$$\nabla \cdot \mathbf{u} = 0 \quad \text{in } \Omega, \tag{2.2}$$

$$\mathbf{u} = \mathbf{0} \quad \text{on } \partial\Omega, \tag{2.3}$$

where  $\mathbf{u}$  and  $p$  denote the velocity and the pressure, respectively.  $S(\mathbf{u}, p)$  is the stress tensor defined as

$$S(\mathbf{u}, p) = 2\mu\boldsymbol{\epsilon}(\mathbf{u}) - p\mathbb{I}, \tag{2.4}$$

where  $\boldsymbol{\epsilon}(\mathbf{u}) = (\nabla\mathbf{u} + (\nabla\mathbf{u})^t)/2$  is the strain tensor, and  $\mathbb{I}$  is the identity tensor. The viscosity function  $\mu(\mathbf{x})$  is assumed to have a finite jump across the interface  $\Gamma$ . For simplicity, we assume that  $\mu(\mathbf{x})$  is a piecewise constant function

$$\mu(\mathbf{x}) = \begin{cases} \mu^- & \text{in } \Omega^-, \\ \mu^+ & \text{in } \Omega^+, \end{cases} \tag{2.5}$$

where  $\mu^\pm$  are positive constants and  $\mathbf{x} = (x, y)$ . Across the fluid interface  $\Gamma$ , the solution is assumed to satisfy the following velocity and stress jump conditions:

$$[[\mathbf{u}]]_\Gamma = 0, \tag{2.6}$$

$$[[S(\mathbf{u}, p)\mathbf{n}]]_\Gamma = \mathbf{0}, \tag{2.7}$$

where the jump  $[[\mathbf{v}(\mathbf{x})]]_\Gamma := \mathbf{v}^+(\mathbf{x})|_\Gamma - \mathbf{v}^-(\mathbf{x})|_\Gamma$ , and  $\mathbf{n}$  denotes the unit normal vector to the interface  $\Gamma$  pointing from  $\Omega^-$  to  $\Omega^+$ . Throughout the paper, we use the standard notation  $(\cdot, \cdot)_\omega$  to denote the  $L^2$  inner product on  $\omega \subset \Omega$ . We omit subscript  $\omega$  if  $\omega = \Omega$ . Note that the Stokes equation (2.1) can be simplified when the viscosity coefficient  $\mu(\mathbf{x})$  is a (piecewise) constant. In this case, the incompressibility condition (2.2) yields

$$\frac{\partial \epsilon_{11}(\mathbf{u})}{\partial x} + \frac{\partial \epsilon_{12}(\mathbf{u})}{\partial y} = \frac{1}{2} \left( \frac{\partial^2 u_1}{\partial x^2} + \frac{\partial}{\partial x} \left( \frac{\partial u_1}{\partial x} + \frac{\partial u_2}{\partial y} \right) + \frac{\partial^2 u_1}{\partial y^2} \right) = \frac{1}{2} \Delta u_1, \tag{2.8}$$

and similarly,

$$\frac{\partial \epsilon_{21}(\mathbf{u})}{\partial x} + \frac{\partial \epsilon_{22}(\mathbf{u})}{\partial y} = \frac{1}{2} \left( \frac{\partial^2 u_2}{\partial x^2} + \frac{\partial}{\partial y} \left( \frac{\partial u_1}{\partial x} + \frac{\partial u_2}{\partial y} \right) + \frac{\partial^2 u_2}{\partial y^2} \right) = \frac{1}{2} \Delta u_2. \tag{2.9}$$

Therefore, the momentum equation (2.1) can be written as

$$-\mu \Delta \mathbf{u} + \nabla p = \mathbf{f} \quad \text{in } \Omega^+ \cup \Omega^-. \tag{2.10}$$

In this framework, the stress interface jump condition (2.7) is modified to

$$[[(\mu \nabla \mathbf{u} - p\mathbb{I})\mathbf{n}]]_\Gamma = \mathbf{0}. \tag{2.11}$$

For more details about derivation of the Stokes equations, we refer the reader to [43].

### 3. CR- $P_0$ immersed finite element space

In this section, we introduce the CR- $P_0$  immersed finite element space for the Stokes interface problem. To this point, we assume that  $\Omega$  is a polygonal domain. Let  $\mathcal{T}_h = \{T_k\}_{k=1}^N$  be an unfitted shape-regular triangulation of  $\Omega$  where  $N = |\mathcal{T}_h|$  denotes the number of triangles. If an element  $T \in \mathcal{T}_h$  is cut through by the interface  $\Gamma$ , we call it an interface element; otherwise, we call it a non-interface element. Denote the collections of interface elements and non-interface elements by  $\mathcal{T}_h^i$  and  $\mathcal{T}_h^n$ , respectively. Let  $\mathcal{E}_h$  be the set of all edges in  $\mathcal{T}_h$ . The collections of interface edges and non-interface edges are denoted by  $\mathcal{E}_h^i$  and  $\mathcal{E}_h^n$ , respectively. The collections of internal edges and boundary edges are denoted by  $\mathcal{E}_h^0$  and  $\mathcal{E}_h^b$ , respectively. Moreover, on a given triangular mesh  $\mathcal{T}_h$ , we assume that it satisfies the following hypotheses:

- **(H1)** The interface can cross at most two edges of an element.
- **(H2)** The interface can cross at most once with each edge, unless the edge is part of the interface.

#### 3.1. CR- $P_0$ FE shape functions

On non-interface elements, the standard CR- $P_0$  finite element functions are used for approximating the velocity and the pressure. Let  $T \in \mathcal{T}_h^n$  be a non-interface element with vertices  $A_1, A_2, A_3$  oriented counterclockwise. We label the edges of  $T$  by  $e_1 = \overline{A_1A_2}$ ,  $e_2 = \overline{A_2A_3}$ , and  $e_3 = \overline{A_3A_1}$ . The degrees of freedom of the CR finite element is determined by the average value over edges. More precisely, the CR local shape functions  $\psi_{j,T} \in P_1, j = 1, 2, 3$  satisfy

$$\frac{1}{|e_i|} \int_{e_i} \psi_{j,T}(x, y) ds = \delta_{ij}, \quad i, j = 1, 2, 3$$

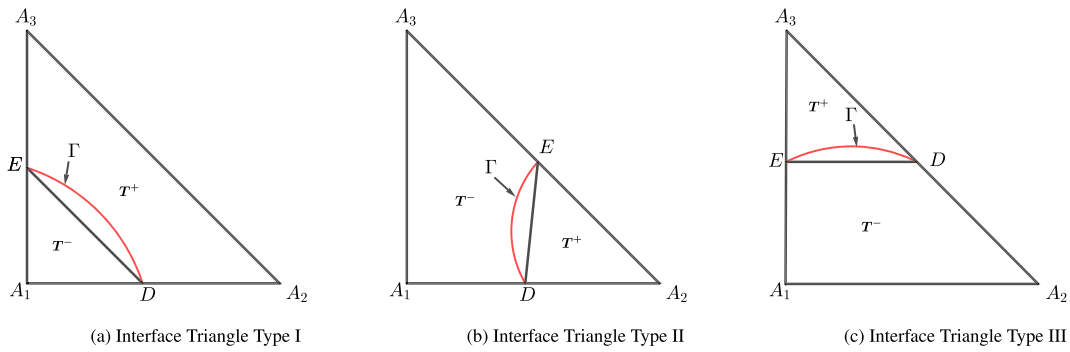


Fig. 2. Types of interface elements. The red curve  $\Gamma$  is the actual interface, and  $\bar{\Gamma}_T = \overline{DE}$  is the line approximation of the interface.

where  $\delta_{ij}$  is the Kronecker function. We approximate the pressure by the piecewise constant function space denoted by  $P_0$ . For the two-dimensional Stokes problem, the components of the velocity and the pressure constitute a vector-valued finite element space, denoted by  $\mathbf{S}_h^n(T) = P_1 \times P_1 \times P_0$ . There are seven local shape functions as follows:

$$\psi_{j,T} = \begin{bmatrix} \psi_{j,T} \\ 0 \\ 0 \end{bmatrix} \text{ for } j = 1, 2, 3, \quad \psi_{j,T} = \begin{bmatrix} 0 \\ \psi_{j-3,T} \\ 0 \end{bmatrix} \text{ for } j = 4, 5, 6, \quad \psi_{7,T} = \begin{bmatrix} 0 \\ 0 \\ 1 \end{bmatrix}. \tag{3.1}$$

The local CR- $P_0$  finite element space can be written as  $\mathbf{S}_h^n(T) = \text{span}\{\psi_{j,T} : 1 \leq j \leq 7\}$ .

### 3.2. CR- $P_0$ IFE shape functions

On an interface element  $T \in \mathcal{T}_h^i$ , simply using polynomial approximations will not be accurate, since the exact solution is not smooth across the interface. We need to modify the functions in  $\mathbf{S}_h^n(T)$  to accommodate the interface jump conditions. Without loss of generality, we consider the following reference triangle  $T$  whose vertices are given by

$$\hat{A}_1 = (0, 0), \quad \hat{A}_2 = (1, 0), \quad \hat{A}_3 = (0, 1).$$

Note that an arbitrary triangle with vertices  $A_i = (x_i, y_i)$ ,  $i = 1, 2, 3$  can be mapped to this reference triangle by the following mapping

$$\begin{bmatrix} \hat{x} \\ \hat{y} \end{bmatrix} = \begin{bmatrix} x_2 - x_1 & x_3 - x_1 \\ y_2 - y_1 & y_3 - y_1 \end{bmatrix}^{-1} \begin{bmatrix} x - x_1 \\ y - y_1 \end{bmatrix}. \tag{3.2}$$

For simplicity, we still use symbols without hat on reference interface elements. Based on the hypotheses (H1) and (H2), there are three geometrical configurations of the interface elements. See Fig. 2 for an illustration. Type I refers to the case where the interface  $\Gamma$  separates  $A_1$  from  $A_2, A_3$ ; Type II refers to the case where the interface  $\Gamma$  separates  $A_2$  from  $A_1, A_3$ ; and Type III refer to the case that the interface  $\Gamma$  separates  $A_3$  from  $A_1, A_2$ . We also let  $D = (x_d, y_d)$  and  $E = (x_e, y_e)$  be the two intersection points of  $\Gamma$  with  $\partial T$ . We use the line segment  $\bar{\Gamma}_T = \overline{DE}$  to approximate the actual interface  $\Gamma_T = \Gamma \cap T$  inside the element. The element  $T$  is subdivided by  $\bar{\Gamma}_T$  into two sub-elements  $T^+$  and  $T^-$ . The intersection points  $D$  and  $E$  can be written as a convex combination of vertices. For instance, for Type I interface elements,  $D = (1 - d)A_1 + dA_2$  and  $E = (1 - e)A_1 + eA_3$  where  $0 < d, e < 1$ .

Now we are ready to construct the local IFE shape functions. Note that for systems of PDEs, the unknown functions are often coupled together through the interface jump conditions. For this Stokes system, the velocity  $\mathbf{u}$  and the pressure  $p$  are coupled together through the stress interface condition (2.7). Thus, vector-valued IFE basis functions must be constructed. Define the following vector-valued IFE shape functions  $\phi_{j,T}$ ,  $1 \leq j \leq 7$  such that  $\phi_{j,T}|_{T^s} = \phi_{j,T}^s = (\phi_{1,j}^s, \phi_{2,j}^s, \phi_{p,j}^s) \in P_1 \times P_1 \times P_0$ , with  $s = +, -$ . To be more explicit, we have

$$\phi_{j,T}(x, y) = \begin{cases} \phi_{j,T}^+(x, y) = \begin{bmatrix} \phi_{1,j}^+(x, y) \\ \phi_{2,j}^+(x, y) \\ \phi_{p,j}^+(x, y) \end{bmatrix} = \begin{bmatrix} a_{1j}^+x + b_{1j}^+y + c_{1j}^+ \\ a_{2j}^+x + b_{2j}^+y + c_{2j}^+ \\ d_j^+ \end{bmatrix}, \\ \phi_{j,T}^-(x, y) = \begin{bmatrix} \phi_{1,j}^-(x, y) \\ \phi_{2,j}^-(x, y) \\ \phi_{p,j}^-(x, y) \end{bmatrix} = \begin{bmatrix} a_{1j}^-x + b_{1j}^-y + c_{1j}^- \\ a_{2j}^-x + b_{2j}^-y + c_{2j}^- \\ d_j^- \end{bmatrix}, \end{cases} \quad j = 1, 2, \dots, 7. \tag{3.3}$$

Each vector-valued IFE shape function  $\phi_{j,T}$  has 14 undetermined coefficients  $a_{1j}^\pm, a_{2j}^\pm, b_{1j}^\pm, b_{2j}^\pm, c_{1j}^\pm, c_{2j}^\pm$ , and  $d_j^\pm$ . These coefficients can be determined by seven local degrees of freedom (average edge values and mean pressure condition), and additional seven interface jump conditions stated below.

- Six edge-value conditions

$$\frac{1}{|e_k|} \int_{e_k} \phi_{j,T} ds = \begin{bmatrix} \delta_{jk} \\ 0 \\ 0 \end{bmatrix}, \quad k = 1, 2, 3, \quad \frac{1}{|e_{k-3}|} \int_{e_{k-3}} \phi_{j,T} ds = \begin{bmatrix} 0 \\ \delta_{jk} \\ 0 \end{bmatrix}, \quad k = 4, 5, 6. \tag{3.4}$$

- One mean pressure condition

$$\frac{1}{|T|} \int_T \phi_{j,T} dx dy = \begin{bmatrix} 0 \\ 0 \\ \delta_{jk} \end{bmatrix}, \quad k = 7. \tag{3.5}$$

- Four continuity conditions of the velocity

$$[\phi_{1,j}(D)] = [\phi_{2,j}(D)] = [\phi_{1,j}(E)] = [\phi_{2,j}(E)] = 0. \tag{3.6}$$

- Two stress continuity conditions

$$[\mu (2\partial_x \phi_{1,j} n_1 + (\partial_y \phi_{1,j} + \partial_x \phi_{2,j}) n_2) - \phi_{p,j} n_1]_{\overline{DE}} = 0, \tag{3.7}$$

$$[\mu ((\partial_x \phi_{2,j} + \partial_y \phi_{1,j}) n_1 + 2\partial_y \phi_{2,j} n_2) - \phi_{p,j} n_2]_{\overline{DE}} = 0. \tag{3.8}$$

- One continuity of the divergence condition

$$[\partial_x \phi_{1,j} + \partial_y \phi_{2,j}]_{\overline{DE}} = 0. \tag{3.9}$$

Combining (3.4)–(3.9) we obtain a  $14 \times 14$  linear system for the Type I interface element:

$$M_1 \mathbf{c}_j = \mathbf{e}_j \tag{3.10}$$

where the coefficient matrix  $M_1$  is given by

$$M_1 = \begin{pmatrix} \frac{1}{2}d^2 & 0 & d & \frac{1-d^2}{2} & 0 & 1-d & 0 & 0 & 0 & 0 & 0 & 0 & 0 & 0 \\ 0 & 0 & 0 & 1/2 & 1/2 & 1 & 0 & 0 & 0 & 0 & 0 & 0 & 0 & 0 \\ 0 & \frac{e^2}{2} & e & 0 & \frac{1-e^2}{2} & 1-e & 0 & 0 & 0 & 0 & 0 & 0 & 0 & 0 \\ 0 & 0 & 0 & 0 & 0 & 0 & d^2/2 & 0 & d & \frac{1-d^2}{2} & 0 & 1-d & 0 & 0 \\ 0 & 0 & 0 & 0 & 0 & 0 & 0 & 0 & 0 & 1/2 & 1/2 & 1 & 0 & 0 \\ 0 & 0 & 0 & 0 & 0 & 0 & 0 & e^2/2 & e & 0 & \frac{1-e^2}{2} & 1-e & 0 & 0 \\ 0 & 0 & 0 & 0 & 0 & 0 & 0 & 0 & 0 & 0 & 0 & 0 & de & 1-de \\ -d & 0 & -1 & d & 0 & 1 & 0 & 0 & 0 & 0 & 0 & 0 & 0 & 0 \\ 0 & -e & -1 & 0 & e & 1 & 0 & 0 & 0 & 0 & 0 & 0 & 0 & 0 \\ 0 & 0 & 0 & 0 & 0 & 0 & -d & 0 & -1 & d & 0 & 1 & 0 & 0 \\ 0 & 0 & 0 & 0 & 0 & 0 & 0 & -e & -1 & 0 & e & 1 & 0 & 0 \\ 2e\mu^- & d\mu^- & 0 & -2e\mu^+ & -d\mu^+ & 0 & d\mu^- & 0 & 0 & -d\mu^+ & 0 & 0 & -e & e \\ 0 & e\mu^- & 0 & 0 & -e\mu^+ & 0 & e\mu^- & 2d\mu^- & 0 & -e\mu^+ & -2d\mu^+ & 0 & -d & d \\ -1 & 0 & 0 & 1 & 0 & 0 & 0 & -1 & 0 & 0 & 1 & 0 & 0 & 0 \end{pmatrix}. \tag{3.11}$$

The unknown vector  $\mathbf{c}_j$  and the right hand side vector  $\mathbf{e}_j$  are

$$\mathbf{c}_j = [a_{1j}^+, b_{1j}^+, c_{1j}^+, a_{1j}^-, b_{1j}^-, c_{1j}^-, a_{2j}^+, b_{2j}^+, c_{2j}^+, a_{2j}^-, b_{2j}^-, c_{2j}^-, d_j^+, d_j^-]^t, \tag{3.12}$$

$$\mathbf{e}_j = [\delta_{j1}, \delta_{j2}, \delta_{j3}, \delta_{j4}, \delta_{j5}, \delta_{j6}, \delta_{j7}, 0, 0, 0, 0, 0, 0, 0]^t. \tag{3.13}$$

With each vector  $\mathbf{e}_j, j = 1, 2, \dots, 7$ , we solve the linear system (3.10) to obtain  $\mathbf{c}_j$ . Substituting the vector  $\mathbf{c}_j$  in (3.3), we obtain the CR- $P_0$  vector-valued IFE shape function  $\phi_{j,T}$ . The derivation of Type II and Type III interface elements are

similar. The coefficient matrix  $M_2$  for Type II interface element is

$$M_2 = \begin{pmatrix} d^2/2 & 0 & d & \frac{1-d^2}{2} & 0 & 1-d & 0 & 0 & 0 & 0 & 0 & 0 & 0 & 0 \\ \frac{1-e^2}{2} & \frac{1-e^2}{2} & 1-e & m_{2,4} & e^2/2 & e & 0 & 0 & 0 & 0 & 0 & 0 & 0 & 0 \\ 0 & 1/2 & 1 & 0 & 0 & 0 & 0 & 0 & 0 & 0 & 0 & 0 & 0 & 0 \\ 0 & 0 & 0 & 0 & 0 & 0 & d^2/2 & 0 & d & \frac{1-d^2}{2} & 0 & 1-d & 0 & 0 \\ 0 & 0 & 0 & 0 & 0 & 0 & m_{5,7} & m_{5,8} & 1-e & m_{5,10} & e^2/2 & e & 0 & 0 \\ 0 & 0 & 0 & 0 & 0 & 0 & 0 & 1/2 & 1 & 0 & 0 & 0 & 0 & 0 \\ 0 & 0 & 0 & 0 & 0 & 0 & 0 & 0 & 0 & 0 & 0 & 0 & m_{7,13} & m_{7,14} \\ -d & 0 & -1 & d & 0 & 1 & 0 & 0 & 0 & 0 & 0 & 0 & 0 & 0 \\ -1+e & -e & -1 & 1-e & e & 1 & 0 & 0 & 0 & 0 & 0 & 0 & 0 & 0 \\ 0 & 0 & 0 & 0 & 0 & 0 & -d & 0 & -1 & d & 0 & 1 & 0 & 0 \\ 0 & 0 & 0 & 0 & 0 & 0 & -1+e & -e & -1 & 1-e & e & 1 & 0 & 0 \\ 2e\mu^- & m_{12,2} & 0 & -2e\mu^+ & m_{12,5} & 0 & m_{12,7} & 0 & 0 & m_{12,10} & 0 & 0 & -e & e \\ 0 & e\mu^- & 0 & 0 & -e\mu^+ & 0 & e\mu^- & m_{13,8} & 0 & -e\mu^+ & m_{13,11} & 0 & m_{13,13} & m_{13,14} \\ -1 & 0 & 0 & 1 & 0 & 0 & 0 & -1 & 0 & 0 & 1 & 0 & 0 & 0 \end{pmatrix} \tag{3.14}$$

where,

$$m_{2,4} = -\frac{1}{2}(-2+e)e, m_{5,7} = m_{2,1}, m_{5,8} = m_{2,2}, m_{5,10} = m_{2,4}, m_{7,13} = 1+(-1+d)e, m_{7,14} = e-de, m_{12,2} = (-1+d+e)\mu^-, m_{13,2} = (-d+e)\mu^-, m_{13,7} = m_{13,2}, m_{12,5} = -(-1+d+e)\mu^+, m_{12,7} = (-1+d+e)\mu^-, m_{12,10} = -(-1+d+e)\mu^+, m_{13,8} = 2(-1+d+e)\mu^-, m_{13,11} = -2(-1+d+e)\mu^+, m_{13,13} = (1-d-e)\mu^+, m_{13,14} = -1+d+e\mu^+.$$

The coefficient matrix  $M_3$  for Type III interface element is

$$M_3 = \begin{pmatrix} 1/2 & 0 & 1 & 0 & 0 & 0 & 0 & 0 & 0 & 0 & 0 & 0 & 0 & 0 \\ m_{2,1} & d^2/2 & d & \frac{(1-d)^2}{2} & \frac{1-d^2}{2} & 1-d & 0 & 0 & 0 & 0 & 0 & 0 & 0 & 0 \\ 0 & e^2/2 & e & 0 & \frac{1-e^2}{2} & 1-e & 0 & 0 & 0 & 0 & 0 & 0 & 0 & 0 \\ 0 & 0 & 0 & 0 & 0 & 0 & 1/2 & 0 & 1 & 0 & 0 & 0 & 0 & 0 \\ 0 & 0 & 0 & 0 & 0 & 0 & m_{5,7} & d^2/2 & d & \frac{(1-d)^2}{2} & \frac{1-d^2}{2} & 1-d & 0 & 0 \\ 0 & 0 & 0 & 0 & 0 & 0 & 0 & e^2/2 & e & 0 & 1-e & 1-e & 0 & 0 \\ 0 & 0 & 0 & 0 & 0 & 0 & 0 & 0 & 0 & 0 & 0 & 0 & m_{7,13} & m_{7,14} \\ -1+d & -d & -1 & 1-d & d & 1 & 0 & 0 & 0 & 0 & 0 & 0 & 0 & 0 \\ 0 & -e & -1 & 0 & e & 1 & 0 & 0 & 0 & 0 & 0 & 0 & 0 & 0 \\ 0 & 0 & 0 & 0 & 0 & 0 & -1+d & -d & -1 & 1-d & d & 1 & 0 & 0 \\ 0 & 0 & 0 & 0 & 0 & 0 & 0 & -e & -1 & 0 & e & 1 & 0 & 0 \\ m_{12,1} & m_{12,2} & 0 & m_{12,4} & m_{12,5} & 0 & m_{12,7} & 0 & 0 & m_{12,10} & 0 & 0 & d-e & -d+e \\ 0 & m_{13,2} & 0 & 0 & m_{13,5} & 0 & m_{13,7} & m_{13,8} & 0 & m_{13,10} & m_{13,11} & 0 & -1+d & 1-d \\ -1 & 0 & 0 & 1 & 0 & 0 & 0 & -1 & 0 & 0 & 1 & 0 & 0 & 0 \end{pmatrix} \tag{3.15}$$

where,

$$m_{2,1} = -\frac{1}{2}(-2+d)d, m_{5,7} = m_{2,1}, m_{7,13} = d+e-de, m_{7,14} = (-1+d)(-1+e), m_{12,1} = 2(-d+e)\mu^-, m_{12,2} = \mu^- - d\mu^-, m_{12,4} = 2(d-e)\mu^+, m_{12,5} = (-1+d)\mu^+, m_{12,7} = \mu^- - d\mu^-, m_{12,10} = (-1+d)\mu^+, m_{13,2} = (-d+e)\mu^-, m_{13,5} = (d-e)\mu^+, m_{13,7} = (-d+e)\mu^-, m_{13,8} = -2(-1+d)\mu^-, m_{13,10} = (d-e)\mu^+, m_{13,11} = 2(-1+d)\mu^+.$$

In Fig. 3, we plot the local CR- $P_0$  IFE vector-valued shape function  $\phi_{3,T}$  and the standard FE vector-valued shape function  $\psi_{3,T}$  as a comparison. There is a kink on all three components of  $\phi_{3,T}$  across the interface, which is designed to satisfy the stress conditions across the interface. Moreover, unlike the FE shape function  $\psi_{3,T}$ , the second and the third components of  $\phi_{3,T}$  are not entirely zero.

We define the local IFE space to be  $\mathbf{S}_h^i(T) = \text{span}\{\phi_{j,T} : 1 \leq j \leq 7\}$ . To unify the notation, we denote the local FE/IFE space on each triangle  $T \in \mathcal{T}_h$  by

$$\mathbf{S}_h(T) = \begin{cases} \mathbf{S}_h^i(T), & \text{if } T \in \mathcal{T}_h^i, \\ \mathbf{S}_h^n(T), & \text{if } T \in \mathcal{T}_h^n. \end{cases} \tag{3.16}$$

The global CR- $P_0$  IFE space is defined to be

$$\mathbf{S}_h(\mathcal{T}_h) = \left\{ \mathbf{v} = [v_1, v_2, v_p]^t \in [L^2(\Omega)]^3 : \mathbf{v}|_T \in \mathbf{S}_h(T), \forall T \in \mathcal{T}_h, \text{ and } \int_e \llbracket v_i \rrbracket ds = 0, \forall e \in \mathcal{E}_h^0, i = 1, 2 \right\}. \tag{3.17}$$

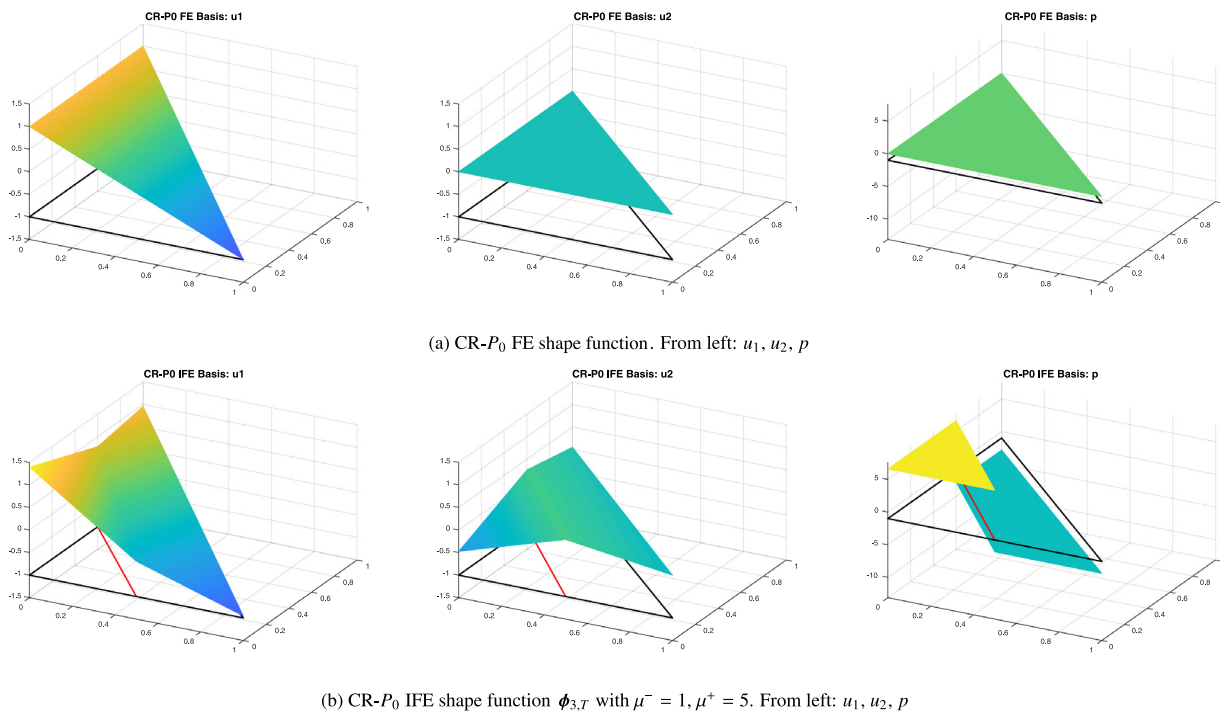


**Fig. 3.** Comparison of the FE shape function  $\psi_{3,T}$  and IFE shape function  $\phi_{3,T}$ .

The subspace with vanishing velocity boundary value is defined as

$$\mathbf{S}_h^0(\mathcal{T}_h) = \left\{ \mathbf{v} = [v_1, v_2, v_p]^t \in \mathbf{S}_h(\mathcal{T}_h) : \int_e v_i ds = 0, \forall e \in \mathcal{E}_h^b, i = 1, 2 \right\}. \tag{3.18}$$

### 4. $RQ_1$ - $Q_0$ immersed finite element space

In this section, we introduce the  $RQ_1$ - $Q_0$  immersed finite element spaces for Stokes interface problem. Let  $\Omega \subset \mathbb{R}^2$  be a rectangular domain or a union of rectangular domains. Assume that  $\Omega$  is partitioned by an interface-unfitted rectangular mesh denoted  $\mathcal{R}_h = \{R_k\}_{k=1}^N$ . As before, we let  $\mathcal{R}_h^i$  and  $\mathcal{R}_h^n$  be the collection of interface elements and non-interface elements, respectively. Define  $\mathcal{E}_h$  to be the set of all edges in  $\mathcal{R}_h$ . Let  $\mathcal{E}_h^i$  and  $\mathcal{E}_h^n$  denote the collection of interface edges and non-interface edges, respectively. The collection of internal edges and boundary edges are denoted by  $\mathcal{E}_h^0$  and  $\mathcal{E}_h^b$ , respectively. In addition, we assume that the rectangular mesh  $\mathcal{R}_h$  satisfies the same hypotheses  $(H_1)$  and  $(H_2)$  as the triangular mesh  $\mathcal{T}_h$ .

#### 4.1. $RQ_1$ - $Q_0$ FE shape functions

We recall the nonconforming rotated- $Q_1$  finite elements which are used to approximate the velocity. Suppose  $R \in \mathcal{R}_h$  is a non-interface element with vertices  $A_1, A_2, A_3, A_4$  which are oriented counterclockwise. The edges of  $R$  are labeled by  $e_1 = A_1A_2, e_2 = A_2A_3, e_3 = A_3A_4,$  and  $e_4 = A_4A_1$ . See the left plot of Fig. 4. The local  $RQ_1$  space is the  $Q_1$  space rotated by  $45^\circ$ , i.e.,

$$RQ_1 = \text{Span}\{1, x, y, x^2 - y^2\}, \tag{4.1}$$

where the local basis functions, denoted by  $\psi_{j,R}$ , satisfy

$$\frac{1}{|e_i|} \int_{e_i} \psi_{j,R}(x, y) ds = \delta_{ij}, \quad i, j = 1, 2, 3, 4,$$

where  $\delta_{ij}$  is the Kronecker function. The pressure is approximated by the piecewise constant function space denoted by  $Q_0$ . The coupled velocity–pressure components create a vector-valued finite element space on each element  $R \in \mathcal{R}_h$ , denoted

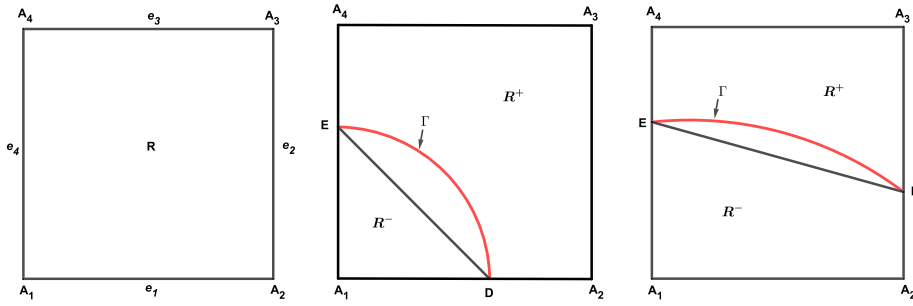


Fig. 4. A noninterface element (left), Type I interface element (middle), and Type II interface element (right).

by  $S_h^n(R) = RQ_1 \times RQ_1 \times Q_0$ . This vector-valued finite element space has nine local shape functions as follows:

$$\psi_{j,R} = \begin{bmatrix} \psi_{j,R} \\ 0 \\ 0 \end{bmatrix} \text{ for } j = 1, 2, 3, 4, \quad \psi_{j,R} = \begin{bmatrix} 0 \\ \psi_{j-4,R} \\ 0 \end{bmatrix} \text{ for } j = 5, 6, 7, 8, \quad \psi_{9,R} = \begin{bmatrix} 0 \\ 0 \\ 1 \end{bmatrix}. \tag{4.2}$$

We can also write the local  $RQ_1$ - $Q_0$  finite element space as  $S_h^n(R) = \text{span}\{\psi_{j,R} : 1 \leq j \leq 9\}$ .

4.2.  $RQ_1$ - $Q_0$  IFE shape functions

Let  $R \in \mathcal{R}_h^i$  be an interface element such that the interface curve  $\Gamma$  intersects  $R$  at the two points, denoted by  $D = (x_d, y_d)$  and  $E = (x_e, y_e)$ . We use the line segment  $\overline{DE}$  to approximate the interface curve within  $R$ . This line segment separates the element  $R$  into two subelements,  $R^+ \in \Omega^+$  and  $R^- \in \Omega^-$ . There are generally two geometrical configurations associated with rectangular interface elements. If the interface intersects an element at two adjacent edge, the element is called a Type I interface element. If the intersection points are on two opposite edges, the element is called a Type II interface element. See Fig. 4.

For simplicity, we present the construction and the analysis of the  $RQ_1$ - $Q_0$  IFE shape functions on a reference element  $\hat{R} = \square\hat{A}_1\hat{A}_2\hat{A}_3\hat{A}_4$ , where

$$\hat{A}_1 = (0, 0), \quad \hat{A}_2 = (1, 0), \quad \hat{A}_3 = (1, 1), \quad \hat{A}_4 = (0, 1).$$

Through straightforward scaling, the reference element  $\hat{R}$  can be mapped to an arbitrary rectangular element  $R$ . We drop the hat for simplicity of the analysis. For the Type I interface element, the intersection points  $D$  and  $E$  can be written as a convex combinations of vertices, i.e.,  $D = (d, 0)$  and  $E = (0, e)$ ; and for Type II interface element  $D = (1, d)$  and  $E = (0, e)$  for  $0 < d, e < 1$ .

Similar to (3.3), we construct  $RQ_1$ - $Q_0$  vector-valued function  $\phi_{j,R}$ , where  $\phi_{j,R} = \phi_{j,R}^s$  on  $R^s$ ,  $s = +, -$  and  $\phi_{j,R}^s = (\phi_{1,j}^s, \phi_{2,j}^s, \phi_{p,j}^s) \in RQ_1 \times RQ_1 \times Q_0$  such that

$$\phi_{j,R}(x, y) = \begin{cases} \phi_{j,R}^+(x, y) = \begin{bmatrix} \phi_{1,j}^+(x, y) \\ \phi_{2,j}^+(x, y) \\ \phi_{p,j}^+(x, y) \end{bmatrix} = \begin{bmatrix} a_{1j}^+ + b_{1j}^+x + c_{1j}^+y + d_{1j}(x^2 - y^2) \\ a_{2j}^+ + b_{2j}^+x + c_{2j}^+y + d_{2j}(x^2 - y^2) \\ d_{pj}^+ \end{bmatrix}, \\ \phi_{j,R}^-(x, y) = \begin{bmatrix} \phi_{1,j}^-(x, y) \\ \phi_{2,j}^-(x, y) \\ \phi_{p,j}^-(x, y) \end{bmatrix} = \begin{bmatrix} a_{1j}^- + b_{1j}^-x + c_{1j}^-y + d_{1j}(x^2 - y^2) \\ a_{2j}^- + b_{2j}^-x + c_{2j}^-y + d_{2j}(x^2 - y^2) \\ d_{pj}^- \end{bmatrix}, \end{cases} \quad j = 1, 2, \dots, 9. \tag{4.3}$$

This linear system has 16 unknowns  $a_{1j}^\pm, a_{2j}^\pm, b_{1j}^\pm, b_{2j}^\pm, c_{1j}^\pm, c_{2j}^\pm, d_{1j}, d_{2j}$ , and  $d_{pj}^\pm$ , which will be determined by the following 16 conditions:

- Eight edge-value conditions

$$\frac{1}{|e_k|} \int_{e_k} \phi_{j,R} ds = \begin{bmatrix} \delta_{jk} \\ 0 \\ 0 \end{bmatrix}, \quad k = 1, 2, 3, 4, \quad \frac{1}{|e_{k-4}|} \int_{e_{k-4}} \phi_{j,R} ds = \begin{bmatrix} 0 \\ \delta_{jk} \\ 0 \end{bmatrix}, \quad k = 5, 6, 7, 8. \tag{4.4}$$

- One mean value condition

$$\frac{1}{|R|} \int_R \phi_{j,R} dx dy = \begin{bmatrix} 0 \\ 0 \\ \delta_{jk} \end{bmatrix}, \quad k = 9. \tag{4.5}$$

- Four velocity conditions across the interface

$$[[\phi_{i,j}(D)]] = [[\phi_{i,j}(E)]] = 0, \quad i = 1, 2. \tag{4.6}$$

- Two weakly imposed stress jump conditions

$$\int_{DE} [[\mu (2\partial_x\phi_{1,j}n_1 + (\partial_y\phi_{1,j} + \partial_x\phi_{2,j})n_2) - \phi_{p,j}n_1]]_{DE} ds = 0, \tag{4.7}$$

$$\int_{DE} [[\mu ((\partial_x\phi_{2,j} + \partial_y\phi_{1,j})n_1 + 2\partial_y\phi_{2,j}n_2) - \phi_{p,j}n_2]]_{DE} ds = 0. \tag{4.8}$$

- One weakly imposed continuity of the divergence condition

$$\int_{DE} [[\partial_x\phi_{1,j} + \partial_y\phi_{2,j}]]_{DE} ds = 0. \tag{4.9}$$

Combining (4.4)–(4.9), we obtain a  $16 \times 16$  linear system:

$$M_i^R \mathbf{c}_j = \mathbf{e}_j, \quad j = 1, 2, \dots, 9, \tag{4.10}$$

where  $M_i^R$ ,  $i = 1, 2$  denote the matrix on Type I and Type II interface element, respectively. Due to the page limit and straightforward formulation, the full matrices  $M_i^R$ ,  $i = 1, 2$  will be omitted in this paper. As before, we choose  $\mathbf{e}_j \in \mathbb{R}^{16}$  to be canonical vectors, and solve for  $\mathbf{c}_j$ , we can obtain the IFE local shape functions  $\phi_{j,R}$ . In Fig. 5, the standard FE vector-valued shape function  $\psi_{3,R}$  and the local IFE vector-valued shape function  $\phi_{3,R}$  are plotted for comparison.

The local  $RQ_1$ - $Q_0$  IFE space on the interface rectangle  $R \in \mathcal{R}_h^i$  is  $\mathbf{S}_h^i(R) = \text{span}\{\phi_{j,R} : 1 \leq j \leq 9\}$ . We also unify the notation by

$$\mathbf{S}_h(R) = \begin{cases} \mathbf{S}_h^i(R), & \text{if } R \in \mathcal{R}_h^i, \\ \mathbf{S}_h^n(R), & \text{if } T \in \mathcal{R}_h^n. \end{cases} \tag{4.11}$$

The global  $RQ_1$ - $Q_0$  IFE space and the zero-boundary subspace are defined to be

$$\mathbf{S}_h(\mathcal{R}_h) = \left\{ \mathbf{v} = [v_1, v_2, v_p]^t \in [L^2(\Omega)]^3 : \mathbf{v}|_T \in \mathbf{S}_h(R), \forall R \in \mathcal{R}_h, \text{ and } \int_e [[v_i]] ds = 0, \forall e \in \mathcal{E}_h^0, i = 1, 2 \right\}. \tag{4.12}$$

$$\mathbf{S}_h^0(\mathcal{R}_h) = \left\{ \mathbf{v} = [v_1, v_2, v_p]^t \in \mathbf{S}_h(\mathcal{R}_h) : \int_e v_i ds = 0, \forall e \in \mathcal{E}_h^b, i = 1, 2 \right\}. \tag{4.13}$$

### 5. Properties of nonconforming IFE spaces

In this section, we present some basic properties of the new nonconforming vector-valued IFE spaces.

**Theorem 5.1** (Unisolvency). *The nonconforming IFE shape functions can be uniquely determined by the prescribed edge values of the velocity and the mean pressure value, regardless the interface locations and the jumps of viscosity coefficients  $\mu^\pm > 0$ . More precisely, we have*

- The  $CR$ - $P_0$  IFE shape functions  $\phi_{j,T}$ ,  $1 \leq j \leq 7$  can be uniquely determined by conditions (3.4)–(3.5)
- The  $RQ_1$ - $Q_0$  IFE shape functions  $\phi_{j,R}$ ,  $1 \leq j \leq 9$  can be uniquely determined by conditions (4.4)–(4.5).

**Proof.** We prove this unisolvency by investigating the invertibility of the coefficient matrices. For the  $CR$ - $P_0$  IFE space, through direct computation, we have

$$\det(M_1) = \frac{1}{16} \left( (1 - de)\mu^- + de\mu^+ \right) (d^2 + e^2)^2 > 0, \tag{5.1}$$

$$\det(M_2) = \frac{1}{16} \left( (1 - d - e)^2 + e^2 \right)^2 \left( \mu^+(1 - e + de) + \mu^-e(1 - d) \right) > 0, \tag{5.2}$$

$$\det(M_3) = \frac{1}{16} \left( (1 - d)^2 + (d - e)^2 \right)^2 \left( \mu^-(1 - d)(1 - e) + \mu^+(d + e(1 - d)) \right) > 0. \tag{5.3}$$

For  $RQ_1$ - $Q_0$  IFE space of Type I interface element, through direct computation we have  $\det(M_1^R) = D_1 + D_2$  where

$$D_1 = \frac{\mu^+}{36} (d^2 + e^2) \left[ de \left( 3(d - e)^2 + 2(d^2 + e^2) \right) \right] > 0$$

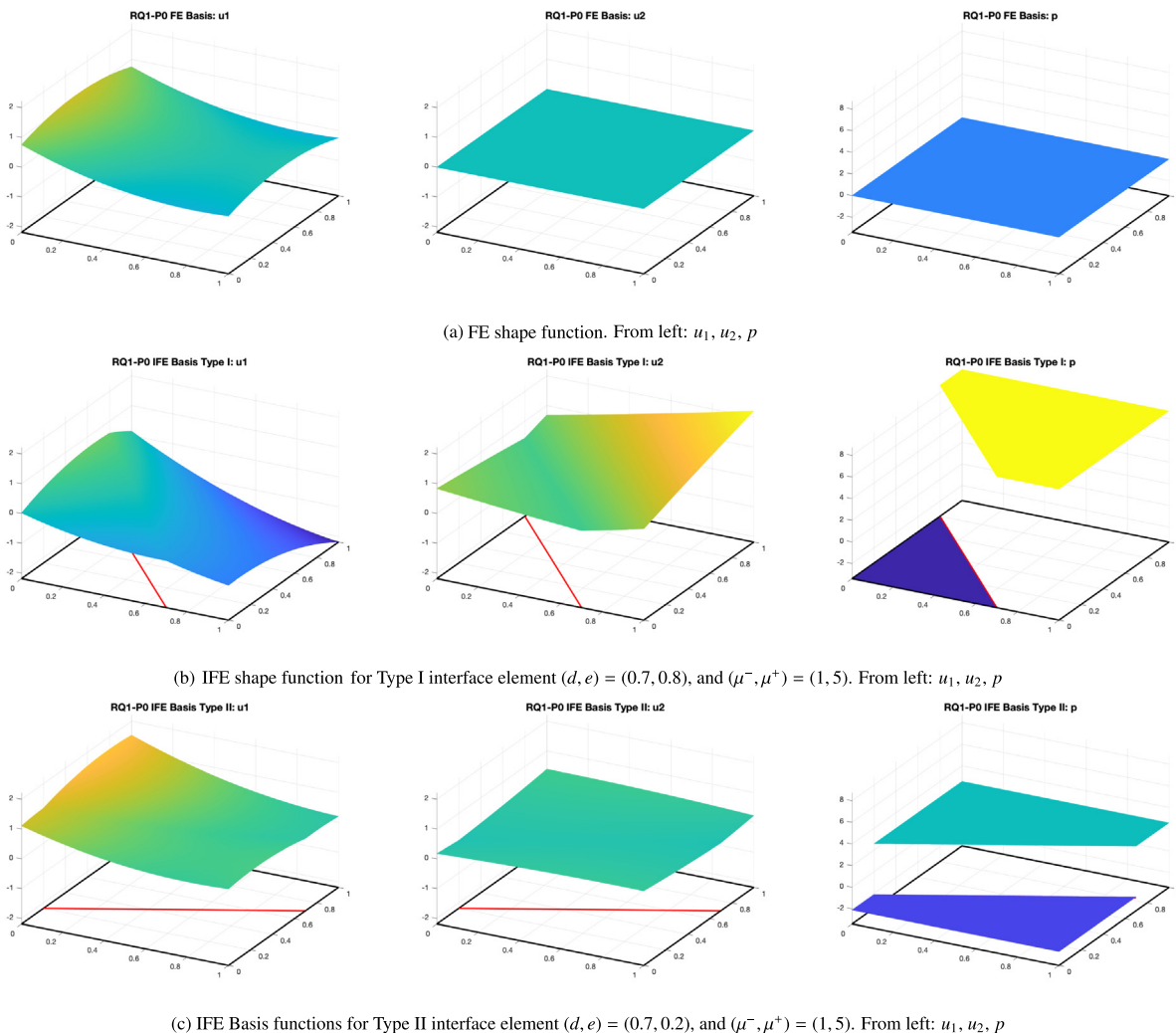


Fig. 5. Comparison of the IFE shape functions (Type I and II)  $\phi_{4,R}$  and the FE shape function  $\psi_{4,R}$ .

$$D_2 = \frac{\mu^-}{36}(d^2 + e^2) \left[ 4d^2 - 5d^3e + 6d^2e^2 + 4e^2 - 5de^3 \right] > \frac{\mu^-}{36}(d^2 + e^2) \left[ d^2(4 - 5e + 3e^2) + e^2(4 - 5d + 3d^2) \right] > 0.$$

For Type II interface element, we have  $\det(M_2^R) = D_3 + D_4$  where

$$D_3 = \frac{\mu^+}{36}(1 + (d - e))^2 \left[ 3d(1 - d)^2 + 3e(1 - e) + d(2 - e)(1 - e) + d(2 - e)(1 - e) + e(2 - d)(1 - d) + 2(d^3 + e^3) \right] > 0,$$

$$D_4 = \frac{\mu^-}{36}(1 + (e - d))^2 \left[ 3(1 - d)d^2 + 3(1 - e)e + (1 - d)(1 - e)e + (1 - e)(1 - d)d + 2((1 - d)^3 + (1 - e)^3) \right] > 0.$$

Thus, both of the CR- $P_0$  and the RQ<sub>1</sub>- $Q_0$  IFE functions of all types are uniquely solvable.  $\square$

**Remark 5.1.** We can use the gradient stress interface condition (2.11) to replace the original stress interface condition (2.7). That is to replace the conditions (3.7)–(3.8) by the following conditions

$$\llbracket \mu (\partial_x \phi_{1,j} n_1 + \partial_y \phi_{1,j} n_2) - \phi_{p,j} n_1 \rrbracket = 0, \tag{5.4}$$

$$\llbracket \mu (\partial_x \phi_{2,j} n_1 + \partial_y \phi_{2,j} n_2) - \phi_{p,j} n_2 \rrbracket = 0, \tag{5.5}$$

in constructing the CR- $P_0$  IFE shape functions. In this case, the new coefficient matrices, denoted by  $\tilde{M}_i$ ,  $i = 1, 2, 3$  are formed by updating the 12th and 13th rows of the matrices  $M_i$ ,  $i = 1, 2, 3$  in (3.11)–(3.15). It is an interesting observation that  $\det(\tilde{M}_i) = \det(M_i)$  for all  $1 \leq i \leq 3$ , although these matrices are not entirely the same. The IFE basis functions using these two stress conditions are very close. Since the determinants are identical, the unisolvency result (Theorem 5.1) also holds true for this configuration. The same results are observed for  $RQ_1$ - $Q_0$  IFE functions.

**Theorem 5.2 (Continuity of Velocity).** *The velocity components of the vector-valued IFE shape functions are continuous within each interface element. To be more accurate,*

- Let  $T \in \mathcal{T}_h^i$  be an interface triangle and let  $\phi_{j,T} = (\phi_{1,j}, \phi_{2,j}, \phi_{p,j})$ ,  $1 \leq j \leq 7$  be the CR- $P_0$  IFE shape functions. Then  $\phi_{i,j} \in C^0(T)$ ,  $i = 1, 2$ .
- Let  $R \in \mathcal{R}_h^i$  be an interface rectangle and let  $\phi_{j,R} = (\phi_{1,j}, \phi_{2,j}, \phi_{p,j})$ ,  $1 \leq j \leq 9$  be the  $RQ_1$ - $Q_0$  IFE shape functions. Then  $\phi_{i,j} \in C^0(R)$ ,  $i = 1, 2$ .

**Proof.** The construction of CR- $P_0$  IFE function uses the velocity jump condition (3.6). Note that two linear functions  $\phi_{i,j}^+$  and  $\phi_{i,j}^-$  coincide along the line segment  $\overline{DE}$  if they match at distinct endpoints  $D$  and  $E$ . This means the velocity components  $\phi_{1,j}$  and  $\phi_{2,j}$  are both continuous across the line segment  $\overline{DE}$ , thus continuous within the whole element  $T$ . For  $RQ_1$ - $Q_0$  IFE function (4.3), since the coefficients of the high-order terms  $x^2 - y^2$  in the velocity components are equal on  $R^+$  and  $R^-$ , their difference is also a linear polynomial. This ensures the continuity of the velocity components over the entire interface element  $R$ .  $\square$

The next two theorems show the consistency of IFE functions with standard FE functions.

**Theorem 5.3 (Consistency I).** *The IFE shape functions become the standard FE shape functions if  $\mu^+ = \mu^-$ . More precisely,*

- Let  $T \in \mathcal{T}_h^i$  be an interface triangle and let  $\phi_{j,T}$ ,  $1 \leq j \leq 7$  be the CR- $P_0$  IFE shape functions. Then  $\phi_{j,T}$  becomes  $\psi_{j,T}$ , if  $\mu^+ = \mu^-$ .
- Let  $R \in \mathcal{R}_h^i$  be an interface rectangle and let  $\phi_{j,R}$ ,  $1 \leq j \leq 9$  be the  $RQ_1$ - $Q_0$  IFE shape functions. Then  $\phi_{j,R}$  becomes  $\psi_{j,R}$ , if  $\mu^+ = \mu^-$ .

**Proof.** It can be verified by direct calculation that when  $\mu^+ = \mu^-$ , the CR- $P_0$  IFE shape functions  $\phi_{j,T}$  become

$$\phi_{1,T}^\pm = \begin{pmatrix} 1 - 2y \\ 0 \\ 0 \end{pmatrix}, \quad \phi_{2,T}^\pm = \begin{pmatrix} 2x + 2y - 1 \\ 0 \\ 0 \end{pmatrix}, \quad \phi_{3,T}^\pm = \begin{pmatrix} 1 - 2x \\ 0 \\ 0 \end{pmatrix}, \tag{5.6}$$

$$\phi_{4,T}^\pm = \begin{pmatrix} 0 \\ 1 - 2y \\ 0 \end{pmatrix}, \quad \phi_{5,T}^\pm = \begin{pmatrix} 0 \\ 2x + 2y - 1 \\ 0 \end{pmatrix}, \quad \phi_{6,T}^\pm = \begin{pmatrix} 0 \\ 1 - 2x \\ 0 \end{pmatrix}, \quad \phi_{7,T}^\pm = \begin{pmatrix} 0 \\ 0 \\ 1 \end{pmatrix}, \tag{5.7}$$

for all three types of the interface configurations. These are exactly the same as standard CR- $P_0$  FE shape functions on the reference triangle. Similar argument can be used for the  $RQ_1$ - $Q_0$  IFE shape functions for all interface types.  $\square$

**Theorem 5.4 (Consistency II).** *The IFE shape functions become the standard FE shape functions if the interface moves out of the element. More precisely,*

- Let  $T \in \mathcal{T}_h^i$  be an interface triangle and let  $\phi_{j,T}$ ,  $1 \leq j \leq 7$  be the CR- $P_0$  IFE shape functions. Then,

$$\phi_{j,T} \rightarrow \psi_{j,T}, \quad \text{as } \frac{\min\{|T^-|, |T^+|\}}{|T|} \rightarrow 0.$$

- Let  $R \in \mathcal{R}_h^i$  be an interface rectangle and let  $\phi_{j,R}$ ,  $1 \leq j \leq 9$  be the  $RQ_1$ - $Q_0$  IFE shape functions. Then,

$$\phi_{j,R} \rightarrow \psi_{j,R}, \quad \text{as } \frac{\min\{|R^-|, |R^+|\}}{|R|} \rightarrow 0.$$

**Proof.** We first consider the CR- $P_0$  IFE case when  $|T^-| \rightarrow 0$ , then

- for Type I element:  $d \rightarrow 0$  or  $e \rightarrow 0$ .
- for Type II element:  $d \rightarrow 0$  and  $e \rightarrow 1$ .
- for Type III element:  $d \rightarrow 0$  and  $e \rightarrow 1$ .

In all the above cases, we have verified by direct calculation that  $\phi_{j,T} \rightarrow \phi_{j,T}^+ = \psi_{j,T}$  for all  $1 \leq j \leq 7$ . Next, if  $|T^+| \rightarrow 0$ , then

- for Type I element:  $d \rightarrow 1$  and  $e \rightarrow 1$ .
- for Type II element:  $d \rightarrow 1$  or  $e \rightarrow 0$ .
- for Type III element:  $d \rightarrow 1$  or  $e \rightarrow 0$ .

In all these cases, we have verified by direct calculation that  $\phi_{j,T} \rightarrow \phi_{j,T}^- = \psi_{j,T}$  for all  $1 \leq j \leq 7$ . Similar argument can be used to verify the consistency for the  $RQ_1-Q_0$  IFE shape functions.  $\square$

The next theorem is concerning the partition of unity property of local IFE shape functions. This property can be verified through direct calculation.

**Theorem 5.5** (Partition of Unity). *The vector-valued IFE functions satisfy the partition of unity property. More precisely,*

- Let  $T \in \mathcal{T}_h^i$  be an interface triangle and let  $\phi_{j,T}, 1 \leq j \leq 7$  be the CR- $P_0$  IFE shape functions. Then

$$\sum_{j=1}^3 \phi_{j,T}(x, y) = \begin{pmatrix} 1 \\ 0 \\ 0 \end{pmatrix}, \quad \sum_{j=4}^6 \phi_{j,T}(x, y) = \begin{pmatrix} 0 \\ 1 \\ 0 \end{pmatrix}, \quad \phi_{7,T}(x, y) = \begin{pmatrix} 0 \\ 0 \\ 1 \end{pmatrix}, \quad \forall (x, y) \in T. \tag{5.8}$$

- Let  $R \in \mathcal{R}_h^i$  be an interface rectangle and let  $\phi_{j,R}, 1 \leq j \leq 9$  be the  $RQ_1-Q_0$  IFE shape functions. Then,

$$\sum_{j=1}^4 \phi_{j,R}(x, y) = \begin{pmatrix} 1 \\ 0 \\ 0 \end{pmatrix}, \quad \sum_{j=5}^8 \phi_{j,R}(x, y) = \begin{pmatrix} 0 \\ 1 \\ 0 \end{pmatrix}, \quad \phi_{9,R}(x, y) = \begin{pmatrix} 0 \\ 0 \\ 1 \end{pmatrix}, \quad \forall (x, y) \in R.$$

**Remark 5.2.** The CR- $P_0$  IFE basis  $\phi_{7,T}$  is a constant vector  $[0, 0, 1]^t$  for any interface location and any coefficient jump. An explanation of this phenomenon is that since the viscosity coefficient  $\mu$  is only a multiple factor of velocity component in (3.7) and (3.8). When the velocity components  $\phi_{1,7} = \phi_{2,7} = 0$ , then the stress interface conditions (3.7) and (3.8) degenerate to  $[[\phi_{p,7}]] = 0$ . Thus, the piecewise constant function  $\phi_{p,7}$  must be continuous within  $T$ , so it must be a constant. The mean-value condition (3.5) further implies that  $\phi_{p,7} = 1$ . Finally, the unisolvent property ensures that  $\phi_{7,T} = [0, 0, 1]^t$  is the only basis to satisfy all edge value conditions. Similar arguments can be applied to conclude  $\phi_{9,R} = [0, 0, 1]^t$ .

### 6. Nonconforming immersed finite element method

In this section, we present the nonconforming CR- $P_0$  IFEM for solving the Stokes interface problem (2.1)–(2.7). First, we derive the weak formulation for the Stokes system.

Multiplying the momentum equation (2.1) by  $\mathbf{v} \in [H_0^1(\Omega)]^2$  and integration by parts over  $\Omega^-$  yields,

$$\int_{\Omega^-} (2\mu\epsilon(\mathbf{u}) - p\mathbb{I}) : \nabla \mathbf{v} \, d\mathbf{x} - \int_{\partial\Omega^-} (2\mu\epsilon(\mathbf{u}) - p\mathbb{I}) \mathbf{n}_{\partial\Omega^-} \cdot \mathbf{v} \, ds = \int_{\Omega^-} \mathbf{f} \cdot \mathbf{v} \, d\mathbf{x}$$

Here the tensor product operator for  $\mathbb{A} = [a_{ij}]$  and  $\mathbb{B} = [b_{ij}]$  is defined to be  $\mathbb{A} : \mathbb{B} \triangleq \sum_{i=1}^n \sum_{j=1}^n a_{ij} b_{ij}$ . Since  $\mathbf{v}$  vanishes on the outer boundary  $\partial\Omega$ , and  $\mathbf{n}_r$  is from  $\Omega^-$  to  $\Omega^+$ , then we have

$$\int_{\Omega^-} (2\mu\epsilon(\mathbf{u}) - p\mathbb{I}) : \nabla \mathbf{v} \, d\mathbf{x} - \int_r (2\mu\epsilon(\mathbf{u}) - p\mathbb{I}) \mathbf{n}_r \cdot \mathbf{v} \, ds = \int_{\Omega^-} \mathbf{f} \cdot \mathbf{v} \, d\mathbf{x}.$$

Similarly on  $\Omega^+$ , we have

$$\int_{\Omega^+} (2\mu\epsilon(\mathbf{u}) - p\mathbb{I}) : \nabla \mathbf{v} \, d\mathbf{x} + \int_r (2\mu\epsilon(\mathbf{u}) - p\mathbb{I}) \mathbf{n}_r \cdot \mathbf{v} \, ds = \int_{\Omega^+} \mathbf{f} \cdot \mathbf{v} \, d\mathbf{x}.$$

Summing up these two equations, we have

$$\int_{\Omega} (2\mu\epsilon(\mathbf{u}) - p\mathbb{I}) : \nabla \mathbf{v} \, d\mathbf{x} - \int_r [(2\mu\epsilon(\mathbf{u}) - p\mathbb{I}) \mathbf{n}_r] \cdot \mathbf{v} \, ds = \int_{\Omega} \mathbf{f} \cdot \mathbf{v} \, d\mathbf{x}.$$

Applying the stress jump condition (2.7), we have

$$\int_{\Omega} (2\mu\epsilon(\mathbf{u}) - p\mathbb{I}) : \nabla \mathbf{v} \, d\mathbf{x} = \int_{\Omega} \mathbf{f} \cdot \mathbf{v} \, d\mathbf{x}.$$

Using the identity  $(2\mu\epsilon(\mathbf{u}) - p\mathbb{I}) : \nabla \mathbf{v} = 2\mu\epsilon(\mathbf{u}) : \epsilon(\mathbf{v}) - p(\nabla \cdot \mathbf{v})$ . Then

$$\int_{\Omega} 2\mu\epsilon(\mathbf{u}) : \epsilon(\mathbf{v}) \, d\mathbf{x} - \int_{\Omega} p(\nabla \cdot \mathbf{v}) \, d\mathbf{x} = \int_{\Omega} \mathbf{f} \cdot \mathbf{v} \, d\mathbf{x}, \tag{6.1}$$

Multiplying a test function  $q \in L^2(\Omega)$  to (2.2), and integration by parts we have

$$\int_{\Omega} q(\nabla \cdot \mathbf{u}) \, d\mathbf{x} = 0 \tag{6.2}$$

At the discretization level, we use the IFE space  $\mathbf{S}_h$  to approximate  $H_0^1(\Omega) \times H_0^1(\Omega) \times L^2(\Omega)$ . The nonconforming CR- $P_0$  or  $RQ_1$ - $Q_0$  IFE method is to find  $(\mathbf{u}_h, p_h) \in \mathbf{S}_h$  such that

$$\begin{aligned} \int_{\Omega} 2\mu \epsilon(\mathbf{u}_h) : \epsilon(\mathbf{v}_h) d\mathbf{x} - \int_{\Omega} p(\nabla \cdot \mathbf{v}_h) d\mathbf{x} &= \int_{\Omega} \mathbf{f} \cdot \mathbf{v}_h d\mathbf{x}, \\ \int_{\Omega} q_h(\nabla \cdot \mathbf{u}_h) d\mathbf{x} &= 0, \end{aligned} \quad \forall (\mathbf{v}_h, q_h) \in \mathbf{S}_h. \tag{6.3}$$

Alternatively, since the viscosity coefficient  $\mu$  is piecewise constant, we can also use the simplified momentum equation (2.10) and the gradient stress condition (2.11). The corresponding IFE method is to find  $(\mathbf{u}_h, p_h) \in \mathbf{S}_h$  such that

$$\begin{aligned} \int_{\Omega} \mu \nabla \mathbf{u}_h : \nabla \mathbf{v}_h d\mathbf{x} - \int_{\Omega} p(\nabla \cdot \mathbf{v}_h) d\mathbf{x} &= \int_{\Omega} \mathbf{f} \cdot \mathbf{v}_h d\mathbf{x}, \\ \int_{\Omega} q_h(\nabla \cdot \mathbf{u}_h) d\mathbf{x} &= 0, \end{aligned} \quad \forall (\mathbf{v}_h, q_h) \in \mathbf{S}_h. \tag{6.4}$$

### 7. Numerical examples

In this section, we test the accuracy and the convergency of the CR- $P_0$  and  $RQ_1$ - $Q_0$  IFE methods for the Stokes interface problem through a series of numerical experiments. We will consider the accuracy of both the interpolation and the IFE solution with various configurations of the interface and coefficient jumps. Interpolation errors and IFE solution errors for the velocity and the pressure are measured by the  $L^2$ - and the broken  $H^1$ -norms.

Define the CR- $P_0$  IFE interpolation operator  $\mathbf{I}_h : H^1(\Omega)^2 \times L^2(\Omega) \rightarrow \mathbf{S}_h(\mathcal{T}_h)$  such that

$$\mathbf{I}_h(\mathbf{u}, p)|_T = \mathbf{I}_{h,T}(\mathbf{u}, p) = \begin{cases} \sum_{j=1}^7 c_j \phi_{j,T}, & \text{if } T \in \mathcal{T}_h^i, \\ \sum_{j=1}^7 c_j \psi_{j,T}, & \text{if } T \in \mathcal{T}_h^n, \end{cases} \tag{7.1}$$

where  $\phi_{j,T}$  and  $\psi_{j,T}$  are the local CR- $P_0$  IFE shape functions and the standard CR- $P_0$  FE shape functions  $T$ , respectively. The coefficients  $c_j$  take the values

$$c_j = \frac{1}{|e_j|} \int_{e_j} u_1(x, y) ds, \quad j = 1, 2, 3, \quad c_j = \frac{1}{|e_{j-3}|} \int_{e_{j-3}} u_2(x, y) ds, \quad j = 4, 5, 6, \quad c_7 = \frac{1}{|T|} \int_T p(x, y) dx dy, \tag{7.2}$$

where  $e_j, j = 1, 2, 3$  are the boundary edges of the triangle  $T$ .

Similarly, the  $RQ_1$ - $Q_0$  IFE interpolation operator  $\mathbf{I}_h : H^1(\Omega)^2 \times L^2(\Omega) \rightarrow \mathbf{S}_h(\mathcal{R}_h)$  is defined to be

$$\mathbf{I}_h(\mathbf{u}, p)|_R = \mathbf{I}_{h,R}(\mathbf{u}, p) = \begin{cases} \sum_{j=1}^9 c_j \phi_{j,R}, & \text{if } R \in \mathcal{R}_h^i, \\ \sum_{j=1}^9 c_j \psi_{j,R}, & \text{if } R \in \mathcal{R}_h^n, \end{cases} \tag{7.3}$$

where  $\phi_{j,R}$  and  $\psi_{j,R}$  are the local  $RQ_1$ - $Q_0$  IFE shape functions and the standard  $RQ_1$ - $Q_0$  FE shape functions  $R$ , respectively. The coefficients  $c_j$  take the values

$$c_j = \frac{1}{|e_j|} \int_{e_j} u_1(x, y) ds, \quad j = 1, 2, 3, 4, \quad c_j = \frac{1}{|e_{j-4}|} \int_{e_{j-4}} u_2(x, y) ds, \quad j = 5, 6, 7, 8, \quad c_9 = \frac{1}{|R|} \int_R p(x, y) dx dy. \tag{7.4}$$

with  $e_j, j = 1, 2, 3, 4$  the boundary edges of the rectangle  $R$ .

Since  $\mathbf{I}_h(\mathbf{u}, p)$  is a vector-valued interpolation, we have the following relations  $(\mathbf{I}_h(\mathbf{u}, p))_1 \approx u_1$ ,  $(\mathbf{I}_h(\mathbf{u}, p))_2 \approx u_2$ , and  $(\mathbf{I}_h(\mathbf{u}, p))_3 \approx p$ . The error of the IFE interpolation for each component is denoted by

$$e_{1,l} = u_1 - \mathbf{I}_h(\mathbf{u}, p)_1, \quad e_{2,l} = u_2 - \mathbf{I}_h(\mathbf{u}, p)_2, \quad e_{p,l} = p - \mathbf{I}_h(\mathbf{u}, p)_3. \tag{7.5}$$

Similarly, the error of the IFE solution for approximating  $u_1, u_2$  and  $p$  are denoted by

$$e_{1,h} = u_1 - u_{1h}, \quad e_{2,h} = u_2 - u_{2h}, \quad e_{p,h} = p - p_h. \tag{7.6}$$

The rate of convergence on two consecutive triangular meshes  $\mathcal{T}_h$  and  $\mathcal{T}_{h/2}$  (or rectangular meshes  $\mathcal{R}_h$  and  $\mathcal{R}_{h/2}$ ) is calculated by

$$r = \frac{\log(e_h/e_{h/2})}{\log(2)}.$$

Numerical examples for the  $RQ_1$ - $Q_0$  IFE method are performed on unfitted Cartesian meshes that contain  $N \times N$  rectangles. For the CR- $P_0$  IFE method, we further divide each rectangle into two triangles by its diagonal with the positive slope. The IFE spaces reported in this paper are based on stress jump conditions (5.4)–(5.5). We also test all numerical examples using the stress conditions (3.7)–(3.8), and the results are very close. We note that these nonconforming

**Table 1**  
Errors of CR- $P_0$  and  $RQ_1$ - $Q_0$  IFE interpolation for Example 1 with  $\mu^- = 1$  and  $\mu^+ = 10$ .

	N	$\ e_{1,I}\ _{L^2(\Omega)}$	Rate	$\ e_{2,I}\ _{L^2(\Omega)}$	Rate	$\ e_{p,I}\ _{L^2(\Omega)}$	Rate	$\ e_{1,I}\ _{H^1(\Omega)}$	Rate	$\ e_{2,I}\ _{H^1(\Omega)}$	Rate
CR	10	7.16e-3	n/a	8.22e-3	n/a	1.71e-1	n/a	1.97e-1	n/a	2.25e-1	n/a
	20	1.80e-3	1.99	2.06e-3	2.00	7.08e-2	1.27	9.87e-2	1.00	1.13e-1	1.00
	40	4.50e-4	2.00	5.15e-4	2.00	3.64e-2	0.96	4.94e-2	1.00	5.64e-2	1.00
	80	1.13e-4	2.00	1.29e-4	2.00	1.80e-2	1.01	2.47e-2	1.00	2.82e-2	1.00
	160	2.82e-5	2.00	3.22e-5	2.00	8.97e-3	1.01	1.24e-2	1.00	1.41e-2	1.00
	320	7.05e-6	2.00	8.05e-6	2.00	4.46e-3	1.01	6.18e-3	1.00	7.06e-3	1.00
$RQ_1$	10	8.39e-3	n/a	1.08e-2	n/a	2.22e-1	n/a	2.06e-1	n/a	2.64e-1	n/a
	20	2.10e-3	2.00	2.70e-3	2.00	1.10e-1	1.02	1.03e-1	1.00	1.32e-1	1.00
	40	5.27e-4	2.00	6.73e-4	2.00	5.50e-2	1.00	5.17e-2	1.00	6.60e-2	1.00
	80	1.32e-4	2.00	1.68e-4	2.00	2.75e-2	1.00	2.59e-2	1.00	3.30e-2	1.00
	160	3.30e-5	2.00	4.21e-5	2.00	1.37e-2	1.00	1.30e-2	1.00	1.65e-2	1.00
	320	8.26e-6	2.00	1.05e-5	2.00	6.87e-3	1.00	6.47e-3	1.00	8.25e-3	1.00

**Table 2**  
Errors of CR- $P_0$  and  $RQ_1$ - $Q_0$  IFE solutions for Example 1 with  $\mu^- = 1$  and  $\mu^+ = 10$ .

	N	$\ e_{1h}\ _{L^2(\Omega)}$	Rate	$\ e_{2h}\ _{L^2(\Omega)}$	Rate	$\ e_{ph}\ _{L^2(\Omega)}$	Rate	$\ e_{1h}\ _{H^1(\Omega)}$	Rate	$\ e_{2h}\ _{H^1(\Omega)}$	Rate
CR	10	1.70e-2	n/a	1.29e-2	n/a	2.20e-1	n/a	2.77e-1	n/a	2.49e-1	n/a
	20	4.24e-3	2.00	3.37e-3	1.94	9.90e-2	1.15	1.40e-1	0.98	1.26e-1	0.98
	40	1.21e-3	1.81	8.95e-4	1.91	5.64e-2	0.81	7.12e-2	0.98	6.35e-2	0.99
	80	2.67e-4	2.18	2.15e-4	2.06	2.41e-2	1.23	3.53e-2	1.01	3.17e-2	1.00
	160	6.70e-5	1.99	5.38e-5	2.00	1.20e-2	1.00	1.76e-2	1.00	1.59e-2	1.00
	320	1.70e-5	1.98	1.34e-5	2.00	6.04e-3	1.00	8.85e-3	1.00	7.93e-3	1.00
$RQ_1$	10	8.07e-3	n/a	1.09e-2	n/a	2.30e-1	n/a	2.27e-1	n/a	2.71e-1	n/a
	20	1.83e-3	2.14	2.70e-3	2.02	1.11e-1	1.05	1.14e-1	1.00	1.36e-1	1.00
	40	6.32e-4	1.53	7.15e-4	1.92	6.21e-2	0.84	5.80e-2	0.97	6.84e-2	0.99
	80	1.14e-4	2.47	1.70e-4	2.08	2.75e-2	1.17	2.85e-2	1.02	3.40e-2	1.01
	160	2.86e-5	1.99	4.23e-5	2.00	1.38e-2	1.00	1.43e-2	1.00	1.70e-2	1.00
	320	7.39e-6	1.95	1.06e-5	1.99	6.90e-3	1.00	7.14e-3	1.00	8.52e-3	1.00

IFE discretizations (6.3) and (6.4) of the Stokes system lead to a saddle-point problem. We use GMRES solver with preconditioners designed by an iterative projection method.

*Example 1 (straight line interface)*

In this example, we consider a Stokes interface problem with a straight line interface. Let  $\Omega = [-1, 1]^2$ , and the interface  $\Gamma = \{(x, y) : y = \frac{\pi}{6}\}$ . The interface divides the domain  $\Omega$  into two subdomains  $\Omega^- = \{(x, y) : y < \frac{\pi}{6}\}$  and  $\Omega^+ = \{(x, y) : y > \frac{\pi}{6}\}$ . Let  $\mu^- = 1$  and  $\mu^+ = 10$ . The exact solutions  $\mathbf{u}$  and  $p$  are chosen as follows:

$$\mathbf{u}(x, y) = \begin{cases} u_1(x, y) = \begin{cases} \frac{1}{\mu^+}(y - \frac{\pi}{6})x^2, & \text{if } (x, y) \in \Omega^+, \\ \frac{1}{\mu^-}(y - \frac{\pi}{6})x^2, & \text{if } (x, y) \in \Omega^-, \end{cases} \\ u_2(x, y) = \begin{cases} -\frac{1}{\mu^+}x(y - \frac{\pi}{6})^2, & \text{if } (x, y) \in \Omega^+, \\ -\frac{1}{\mu^-}x(y - \frac{\pi}{6})^2, & \text{if } (x, y) \in \Omega^-, \end{cases} \end{cases} \quad p(x, y) = e^x - e^y. \tag{7.7}$$

In Table 1, we present the errors and the convergence rates of the IFE interpolations. It can be seen that the convergence rates for velocity components  $u_1$  and  $u_2$  are  $\mathcal{O}(h^2)$  in the  $L^2$ -norm and  $\mathcal{O}(h)$  in the broken  $H^1$ -norm. Convergence rates for the pressure  $p$  is  $\mathcal{O}(h)$  in the  $L^2$ -norm. This result is consistent with our expectation based on the degrees of polynomials we used for the approximation. In Table 2, we report the errors and the convergence rates for the IFE solution. The convergence rates for all the norms mentioned above are optimal.

*Example 2 (curved interface)*

In this example, we consider a circular interface problem which has been used in Example 4.2 in [34]. Let  $\Omega = [-1, 1]^2$  and the interface  $\Gamma = \{(x, y) : x^2 + y^2 = 0.3\}$ . The circular interface separates the domain  $\Omega$  into two subdomains  $\Omega^- = \{(x, y) : x^2 + y^2 < 0.3\}$  and  $\Omega^+ = \{(x, y) : x^2 + y^2 > 0.3\}$ . Let  $\mu^- = 1$  and  $\mu^+ = 10$ . The exact solutions  $\mathbf{u} = [u_1, u_2]^t$  and  $p$  are chosen as follows:

$$u_1 = \begin{cases} \frac{y(x^2+y^2-0.3)}{\mu^+}, & \text{if } (x, y) \in T^+, \\ \frac{y(x^2+y^2-0.3)}{\mu^-}, & \text{if } (x, y) \in T^-, \end{cases} \quad u_2 = \begin{cases} \frac{-x(x^2+y^2-0.3)}{\mu^+}, & \text{if } (x, y) \in T^+, \\ \frac{-x(x^2+y^2-0.3)}{\mu^-}, & \text{if } (x, y) \in T^-, \end{cases} \tag{7.8}$$

**Table 3**  
Errors of CR- $P_0$  and  $RQ_1$ - $Q_0$  IFE interpolation for Example 2 with  $\mu^- = 1, \mu^+ = 10$ .

	N	$\ e_{1,I}\ _{L^2(\Omega)}$	Rate	$\ e_{2,I}\ _{L^2(\Omega)}$	Rate	$\ e_{p,I}\ _{L^2(\Omega)}$	Rate	$\ e_{1,I}\ _{H^1(\Omega)}$	Rate	$\ e_{2,I}\ _{H^1(\Omega)}$	Rate
CR	10	3.36e-3	n/a	3.36e-3	n/a	4.00e-2	n/a	9.02e-2	n/a	9.06e-2	n/a
	20	9.01e-4	1.90	9.01e-4	1.90	1.29e-2	1.63	4.59e-2	0.97	4.61e-2	0.97
	40	2.34e-4	1.94	2.34e-4	1.94	6.85e-3	0.92	2.36e-2	0.96	2.36e-2	0.97
	80	5.94e-5	1.98	5.94e-5	1.98	2.77e-3	1.31	1.21e-2	0.96	1.20e-2	0.98
	160	1.49e-5	1.99	1.49e-5	1.99	1.19e-3	1.22	6.01e-3	1.01	5.94e-3	1.02
	320	3.74e-6	1.99	3.74e-6	1.99	5.32e-4	1.16	2.98e-3	1.01	2.95e-3	1.01
$RQ_1$	10	4.11e-3	n/a	4.11e-3	n/a	2.17e-2	n/a	1.07e-1	n/a	1.07e-1	n/a
	20	1.04e-3	1.98	1.04e-3	1.04	1.10e-2	0.98	5.17e-2	1.06	5.16e-2	1.06
	40	2.69e-4	1.95	2.69e-4	1.95	5.48e-3	1.00	2.68e-2	0.95	2.68e-2	0.95
	80	6.74e-5	2.00	6.74e-5	2.00	2.74e-3	1.00	1.36e-2	0.97	1.37e-2	0.97
	160	1.68e-5	2.00	1.68e-5	2.00	1.37e-3	1.00	6.72e-3	1.02	6.73e-3	1.02
	320	4.20e-6	2.00	4.20e-6	2.00	6.85e-4	1.00	3.33e-3	1.01	3.33e-3	1.01

**Table 4**  
Errors of CR- $P_0$  and  $RQ_1$ - $Q_0$  IFE solution for Example 2 with  $\mu^- = 1, \mu^+ = 10$ .

	N	$\ e_{1h}\ _{L^2(\Omega)}$	Rate	$\ e_{2h}\ _{L^2(\Omega)}$	Rate	$\ e_{ph}\ _{L^2(\Omega)}$	Rate	$\ e_{1h}\ _{H^1(\Omega)}$	Rate	$\ e_{2h}\ _{H^1(\Omega)}$	Rate
CR	10	4.20e-3	n/a	4.20e-3	n/a	7.60e-2	n/a	1.02e-1	n/a	1.02e-1	n/a
	20	1.14e-3	1.88	1.14e-3	1.88	3.24e-2	1.23	5.31e-2	0.93	5.33e-2	0.94
	40	2.96e-4	1.94	2.96e-4	1.94	1.60e-2	1.03	2.75e-2	0.95	2.75e-2	0.96
	80	7.62e-5	1.96	7.62e-5	1.96	7.53e-3	1.09	1.41e-2	0.96	1.40e-2	0.97
	160	1.91e-5	1.99	1.91e-5	1.99	3.66e-3	1.04	7.03e-3	1.00	6.98e-3	1.01
	320	4.81e-6	1.99	4.81e-6	1.99	1.80e-3	1.03	3.50e-3	1.01	3.48e-3	1.00
$RQ_1$	10	4.88e-3	n/a	4.88e-3	n/a	4.25e-2	n/a	1.05e-1	n/a	1.05e-1	n/a
	20	1.13e-3	2.11	1.13e-3	2.11	1.46e-2	1.54	5.13e-2	1.04	5.13e-2	1.04
	40	2.97e-4	1.93	2.97e-4	1.93	6.36e-3	1.20	2.68e-2	0.94	2.68e-2	0.94
	80	7.80e-5	1.93	7.80e-5	1.93	2.90e-3	1.13	1.36e-2	0.97	1.36e-2	0.97
	160	1.91e-5	2.03	1.91e-5	2.03	1.41e-3	1.04	6.71e-3	1.02	6.73e-3	1.02
	320	4.74e-6	2.01	4.74e-6	2.01	6.93e-4	1.02	3.33e-3	1.01	3.33e-3	1.01

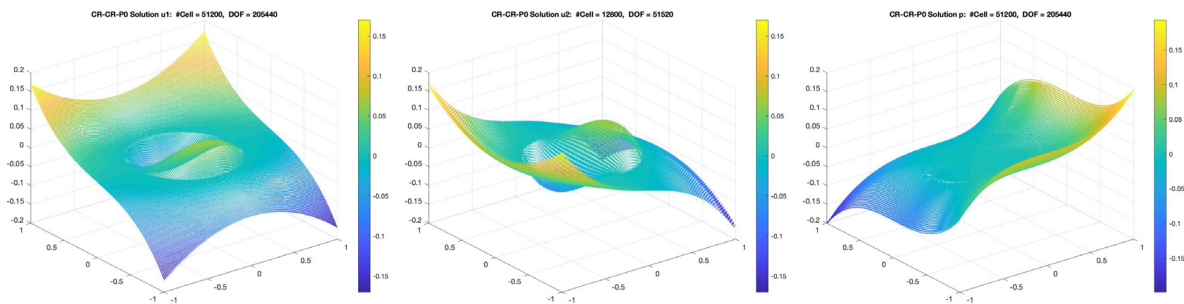


**Fig. 6.** IFE solutions  $u_{1h}, u_{2h},$  and  $p_h$  on the  $160 \times 160$  mesh of Example 2 with  $\mu^- = 1, \mu^+ = 10$ .

and

$$p = \frac{1}{10}(x^3 - y^3). \tag{7.9}$$

Errors of the IFE interpolation and the IFE solution for this problem are reported in Tables 3 and 4, respectively. Again, the convergence rates for both the interpolation and the IFE solution are optimal in all norms. The CR- $P_0$  IFE solution on the  $160 \times 160$  mesh is plotted in Fig. 6. One can observe that the numerical solution around interface circle is resolved accurately. The velocity vector field is plotted in the left plot of Fig. 7.

*Example 3 (flipped coefficients and large coefficient contrast)*

In this example, we consider the curved interface problem in Example 2 again with different jump ratios. This time we only report the IFE solution errors in consideration of the page limit. The convergence rates of the IFE interpolation are optimal as usual. In Tables 5 and 6 we report the error of IFE solutions for the case when the coefficient is flipped ( $\mu^-, \mu^+ = 10, 1$ ), and when the coefficient has a large jump ( $\mu^-, \mu^+ = 1, 1000$ ), respectively. As before, we can see that the convergence rates are optimal for both cases. In Fig. 7, we plot the velocity vector field of these cases.

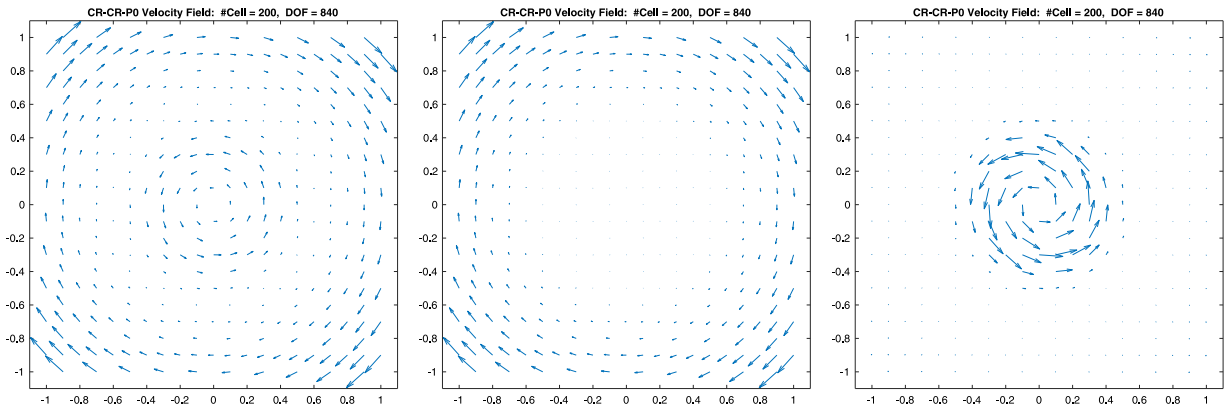


Fig. 7. Velocity vector field of Example 2 and Example 3 with various coefficients. From left:  $(\mu^-, \mu^+) = (1, 10)$ ,  $(10, 1)$ , and  $(1, 1000)$ .

Table 5

Errors of CR- $P_0$  and  $RQ_1$ - $Q_0$  IFE solution for Example 3 with  $\mu^- = 10$ ,  $\mu^+ = 1$ .

	N	$\ e_{1h}\ _{L^2(\Omega)}$	Rate	$\ e_{2h}\ _{L^2(\Omega)}$	Rate	$\ e_{ph}\ _{L^2(\Omega)}$	Rate	$\ e_{1h}\ _{H^1(\Omega)}$	Rate	$\ e_{2h}\ _{H^1(\Omega)}$	Rate
CR	10	1.88e-2	n/a	1.88e-2	n/a	6.84e-2	n/a	4.27e-1	n/a	4.27e-1	n/a
	20	4.85e-3	1.96	4.85e-3	1.96	3.71e-2	0.88	2.15e-1	0.99	2.16e-1	0.99
	40	1.22e-3	1.99	1.22e-3	1.99	1.62e-2	1.20	1.08e-1	0.99	1.08e-1	0.99
	80	3.07e-4	1.99	3.07e-4	1.99	7.38e-3	1.13	5.43e-2	1.00	5.42e-2	1.00
	160	7.69e-5	2.00	7.69e-5	2.00	3.63e-3	1.02	2.71e-2	1.00	2.71e-2	1.00
	320	1.92e-5	2.00	1.92e-5	2.00	1.79e-3	1.02	1.36e-2	1.00	1.36e-2	1.00
$RQ_1$	10	1.21e-2	n/a	1.21e-2	n/a	2.56e-2	n/a	4.10e-1	n/a	4.10e-1	n/a
	20	3.06e-3	1.98	3.06e-3	1.98	1.51e-2	0.76	2.05e-1	1.00	2.05e-1	1.00
	40	7.74e-4	1.98	7.74e-4	1.98	6.00e-3	1.33	1.03e-1	1.00	1.03e-1	1.00
	80	1.94e-4	1.99	1.94e-4	1.99	2.93e-3	1.04	5.14e-2	1.00	5.15e-2	1.00
	160	4.84e-5	2.01	4.84e-5	2.01	1.42e-3	1.05	2.57e-2	1.00	2.57e-2	1.00
	320	1.21e-5	2.00	1.21e-5	2.00	6.97e-4	1.02	1.28e-2	1.00	1.28e-2	1.00

Table 6

Errors of CR- $P_0$  and  $RQ_1$ - $Q_0$  IFE solution for Example 3 with  $\mu^- = 1$ ,  $\mu^+ = 1000$ .

	N	$\ e_{1h}\ _{L^2(\Omega)}$	Rate	$\ e_{2h}\ _{L^2(\Omega)}$	Rate	$\ e_{ph}\ _{L^2(\Omega)}$	Rate	$\ e_{1h}\ _e - H^1(\Omega)$	Rate	$\ e_{2h}\ _{H^1(\Omega)}$	Rate
CR	10	1.22e-2	n/a	1.22e-2	n/a	8.27e-1	n/a	1.35e-1	n/a	1.36e-1	n/a
	20	2.37e-3	2.36	2.37e-3	2.36	6.39e-1	0.37	5.56e-2	1.28	5.58e-2	1.28
	40	5.58e-4	2.09	5.58e-4	2.09	3.43e-1	0.90	2.64e-2	1.08	2.64e-2	1.08
	80	1.10e-4	2.34	1.10e-4	2.34	1.37e-1	1.32	1.32e-2	0.99	1.31e-2	1.01
	160	2.25e-5	2.29	2.25e-5	2.29	4.96e-2	1.47	6.56e-3	1.01	6.49e-3	1.02
	320	4.87e-6	2.21	4.87e-6	2.21	1.73e-2	1.52	3.24e-3	1.02	3.21e-3	1.01
$RQ_1$	10	1.90e-2	n/a	1.90e-2	n/a	9.75e-1	n/a	1.70e-1	n/a	1.70e-1	n/a
	20	3.19e-3	2.57	3.19e-3	2.57	6.02e-1	0.69	5.54e-2	1.62	5.53e-2	1.62
	40	1.35e-3	1.24	1.35e-3	1.24	2.57e-1	1.23	3.07e-2	0.85	3.07e-2	0.85
	80	2.20e-4	2.62	2.20e-4	2.62	1.01e-1	1.35	1.33e-2	1.20	1.34e-2	1.20
	160	3.47e-5	2.66	3.47e-5	2.66	3.58e-2	1.49	6.35e-3	1.07	6.37e-3	1.07
	320	6.45e-6	2.43	6.45e-6	2.43	1.30e-2	1.46	3.10e-3	1.06	3.11e-3	1.04

### 8. Conclusion

In this paper, we introduced two low-order nonconforming immersed finite element methods for Stokes interface problems. The CR- $P_0$  and  $RQ_1$ - $Q_0$  IFE approximations can be used on interface-unfitted triangular and rectangular meshes, respectively. The vector-valued IFE space is constructed to approximate the velocity and stress jump conditions across the interface. Basic properties such as the unsolvency and the partition of unity of the IFE space are proved. Numerical experiments are carried out to demonstrate the optimal convergence of both IFE interpolations and the IFE solutions for small and large viscosity contrasts.

### Acknowledgments

Derrick Jones was partially supported by the National Science Foundation Graduate Research Fellowship, USA NO. 1645630. Xu Zhang was partially supported by the National Science Foundation, USA (Grant Numbers DMS-1720425 and DMS-2005272). The authors would like to thank Xiaozhe Hu for valuable communications.

## References

- [1] I. Babuska, The finite element method for elliptic equations with discontinuous coefficients, *Computing* 5 (1970) 207–213.
- [2] I. Babuska, J.E. Osborn, Can a finite element method perform arbitrarily badly? *Math. Comp.* 69 (230) (2000) 443–462.
- [3] Z. Li, The immersed interface method using a finite element formulation, *Appl. Numer. Math.* 27 (3) (1998) 253–267.
- [4] S. Adjerid, T. Lin, A  $p$ -th degree immersed finite element for boundary value problems with discontinuous coefficients, *Appl. Numer. Math.* 59 (6) (2009) 1303–1321.
- [5] W. Cao, X. Zhang, Z. Zhang, Superconvergence of immersed finite element methods for interface problems, *Adv. Comput. Math.* 43 (4) (2017) 795–821.
- [6] D. Jones, X. Zhang, A high order immersed finite element method for parabolic interface problems, in: *ITM Web of Conferences*, vol. 29, 2019, p. 01007.
- [7] R. Guo, T. Lin, A higher degree immersed finite element method based on a Cauchy extension for elliptic interface problems, *SIAM J. Numer. Anal.* 57 (4) (2019) 1545–1573.
- [8] C. He, X. Zhang, Residual-based a posteriori error estimation for immersed finite element methods, *J. Sci. Comput.* 81 (3) (2019) 2051–2079.
- [9] X. He, T. Lin, Y. Lin, Approximation capability of a bilinear immersed finite element space, *Numer. Methods Partial Differential Equations* 24 (5) (2008) 1265–1300.
- [10] X. He, T. Lin, Y. Lin, Immersed finite element methods for elliptic interface problems with non-homogeneous jump conditions, *Int. J. Numer. Anal. Model.* 8 (2) (2011) 284–301.
- [11] T. Lin, Y. Lin, X. Zhang, Partially penalized immersed finite element methods for elliptic interface problems, *SIAM J. Numer. Anal.* 53 (2) (2015) 1121–1144.
- [12] S. Vallaghé, T. Papadopoulou, A trilinear immersed finite element method for solving the electroencephalography forward problem, *SIAM J. Sci. Comput.* 32 (4) (2010) 2379–2394.
- [13] T. Lin, Q. Yang, X. Zhang, Partially penalized immersed finite element methods for parabolic interface problems, *Numer. Methods Partial Differential Equations* 31 (6) (2015) 1925–1947.
- [14] T. Lin, Q. Zhuang, Optimal error bounds for partially penalized immersed finite element methods for parabolic interface problems, *J. Comput. Appl. Math.* 366 (11) (2020) 112401.
- [15] S. Adjerid, K. Moon, An immersed discontinuous Galerkin method for acoustic wave propagation in inhomogeneous media, *SIAM J. Sci. Comput.* 41 (1) (2019) A139–A162.
- [16] T. Lin, Y. Lin, Q. Zhuang, Solving interface problems of the Helmholtz equation by immersed finite element methods, *Commun. Appl. Math. Comput.* 1 (2) (2019) 187–206.
- [17] R. Guo, T. Lin, Y. Lin, A fixed mesh method with immersed finite elements for solving interface inverse problems, *J. Sci. Comput.* 79 (1) (2019) 148–175.
- [18] R. Guo, T. Lin, Y. Lin, Recovering elastic inclusions by shape optimization methods with immersed finite elements, *J. Comput. Phys.* 404 (24) (2020) 109123.
- [19] R. Guo, T. Lin, Y. Lin, Error estimates for a partially penalized immersed finite element method for elasticity interface problems, *ESAIM Math. Model. Numer. Anal.* 54 (1) (2020) 1–24.
- [20] T. Lin, X. Zhang, Linear and bilinear immersed finite elements for planar elasticity interface problems, *J. Comput. Appl. Math.* 236 (18) (2012) 4681–4699.
- [21] T. Lin, D. Sheen, X. Zhang, A locking-free immersed finite element method for planar elasticity interface problems, *J. Comput. Phys.* 247 (2013) 228–247.
- [22] S. Adjerid, N. Chaabane, T. Lin, P. Yue, An immersed discontinuous finite element method for the Stokes problem with a moving interface, *J. Comput. Appl. Math.* 362 (2019) 540–559.
- [23] X. He, T. Lin, Y. Lin, X. Zhang, Immersed finite element methods for parabolic equations with moving interface, *Numer. Methods Partial Differential Equations* 29 (2) (2013) 619–646.
- [24] Y. Chen, S. Hou, X. Zhang, An immersed finite element method for elliptic interface problems with multi-domain and triple junction points, *Adv. Appl. Math. Mech.* 11 (5) (2019) 1005–1021.
- [25] Y. Chen, S. Hou, X. Zhang, A bilinear partially penalized immersed finite element method for elliptic interface problems with multi-domains and triple-junction points, *Results Appl. Math.* 8 (2020) 100100.
- [26] J. Bai, Y. Cao, Y. Chu, X. Zhang, An improved immersed finite element particle-in-cell method for plasma simulation, *Comput. Math. Appl.* 75 (6) (2018) 1887–1899.
- [27] Y. Cao, Y. Chu, X. He, T. Lin, An iterative immersed finite element method for an electric potential interface problem based on given surface electric quantity, *J. Comput. Phys.* 281 (2015) 82–95.
- [28] P. Hansbo, M.G. Larson, S. Zahedi, A cut finite element method for a Stokes interface problem, *Appl. Numer. Math.* 85 (2014) 90–114.
- [29] N. Wang, J. Chen, A nonconforming Nitsche's extended finite element method for Stokes interface problems, *J. Sci. Comput.* 81 (1) (2019) 342–374.
- [30] S. Großand, A. Reusken, An extended pressure finite element space for two-phase incompressible flows with surface tension, *J. Comput. Phys.* 224 (1) (2007) 40–58.
- [31] A. Lundberg, P. Sun, C. Wang, Distributed Lagrange multiplier-fictitious domain finite element method for Stokes interface problems, *Int. J. Numer. Anal. Model.* 16 (6) (2019) 939–963.
- [32] P. Sun, Fictitious domain finite element method for Stokes/elliptic interface problems with jump coefficients, *J. Comput. Appl. Math.* 356 (2019) 81–97.
- [33] Z. Li, K. Ito, M.-C. Lai, An augmented approach for Stokes equations with a discontinuous viscosity and singular forces, *Comput. & Fluids* 36 (3) (2007) 622–635.
- [34] S. Adjerid, N. Chaabane, T. Lin, An immersed discontinuous finite element method for Stokes interface problems, *Comput. Methods Appl. Mech. Engrg.* 293 (2015) 170–190.
- [35] M. Crouzeix, P.-A. Raviart, Conforming and nonconforming finite element methods for solving the stationary Stokes equations I, *R.A.I.R.O.* 7 (1973) 33–75.
- [36] R. Rannacher, S. Turek, Simple nonconforming quadrilateral Stokes element, *Numer. Methods Partial Differential Equations* 8 (2) (1992) 97–111.
- [37] D.N. Arnold, On nonconforming linear-constant elements for some variants of the Stokes equations, *Istit. Lombardo Accad. Sci. Lett. Rend. A* 127 (1993) 83–93.
- [38] J. Li, Z. Chen, A new local stabilized nonconforming finite element method for the Stokes equations, *Computing* 82 (2–3) (2008) 157–170.
- [39] C. Taylor, P. Hood, A numerical solution of the Navier-Stokes equations using the finite element technique, *Int. J. Comput. Fluids* 1 (1) (1973) 73–100.
- [40] Z. Chen, Finite element methods and their applications, in: *Scientific Computation*, Springer-Verlag, Berlin, 2005.

- [41] T. Lin, D. Sheen, X. Zhang, A nonconforming immersed finite element method for elliptic interface problems, *J. Sci. Comput.* 79 (1) (2019) 442–463.
- [42] R. Guo, T. Lin, X. Zhang, Nonconforming immersed finite element spaces for elliptic interface problems, *Comput. Math. Appl.* 75 (6) (2018) 2002–2016.
- [43] V. Girault, P.-A. Raviart, Finite element approximation of the Navier-Stokes equations, in: *Lecture Notes in Mathematics*, vol. 749, Springer-Verlag, Berlin-New York, 1979.